ORIGAMI INSPIRED DESIGN OF THIN WALLED TUBULAR STRUCTURES FOR IMPACT LOADING

A Thesis

Submitted to the Faculty

of

Purdue University

by

Shantanu R. Shinde

In Partial Fulfillment of the

Requirements for the Degree

of

Master of Science in Mechanical Engineering

August 2019

Purdue University

Indianapolis, Indiana

THE PURDUE UNIVERSITY GRADUATE SCHOOL
STATEMENT OF COMMITTEE APPROVAL

Dr. Andres Tovar, Chair

Department of Mechanical and Energy Engineering

Dr. Khosrow Nematollahi

Department of Mechanical and Energy Engineering

Dr. Hamid Dalir

Department of Mechanical and Energy Engineering

Approved by:

Dr. Sohel Anwar

Chair of the Graduate Program

To my family.

ACKNOWLEDGMENTS

The work reported in this thesis was conducted in the Engineering Design Research Lab at the Purdue School of Engineering & Technology, Indianapolis. I received a lot of help from many people during my time there, without whom I would have not been able to complete my research work.

The first and most important person I would like to thank is my advisor, Dr.Tovar, who introduced me to the field of crashworthiness. He inspired, motivated and always supported me from the very beginning to the end. His broad knowledge in the related fields helped me a lot in solving the problems I faced during my research work.

My special thanks to my members of the committe, Dr. Khosrow Nematollahi, whose courses, FEM and Advanced FEM for solids, greatly broadened and enhanced my understating of Finite Element Methods and structural dynamics and Dr. Hamid Dalir, whose invaluable suggestions help a lot in improving the thesis.

I would like to thank my friends, Akshay Dalvi, Ashwin Gaonkar, Abhishek Kawade, Shashank Alai, Niraj Kumbhare, Vikhil Desai and Atish Dahitule for always supporting and motivating me.

I would also like to thank my fellow members at EDRL, Joel Najmon, Homero Valladares-Guerra, Kai Liu, Sajjad Raeisi, Prasad Tapkir and Prathamesh Chaudhari for their help and encouragement.

Financial support from ITEC scholarship and FORCES grant is gratefully acknowledged. I would like to thank Dr. Tovar for believing and nominating me for these funding opportunities.

Finally, I would like to thank my father, mother and my brother, you loved and supported me unconditionally.

TABLE OF CONTENTS

Page

Page

LIST OF TABLES

LIST OF FIGURES

Figure Page

SYMBOLS

b	width of square tube
c	width of the lobe
C, p	Material constants (Cowper-Symonds equation)
D	duameter of circular tube
E	Youngs's Modulus
g	acceleration due to gravity
I	moment of inertia of a cross section
l	length of the unfolded module
m	mass
M	number of modules
n	power law exponent
P_E	Euler buckling force
P_m	mean crushing force
P_{max}	peak crushing force
t	wall thickness
V	velocity
δ	crushing distance
δ_1	Amplitude of half sine component of thr curve pre-folded on the strut
δ_2	Amplitude of full sine component of thr curve pre-folded on the strut
δ_m	max deflection in a strut
δ_y	deflection to cause yield in a strut
Δt	time step increment

$\dot{\epsilon}$	strain rate
2θ	dihedral angle
μ	coefficient of friction
ρ	material density
σ_y	yield stress
σ_u	ultimate stress
σ_o	plastic flow stress
σ_o^d	dynamic plastic flow stress
χ	Curvature of strut

ABBREVIATIONS

SEA	Specific Energy Absorption
EA	Energy Absorption
CFE	Crush Force Efficiency
ms	*millisecond*
kN	Kilo Newton
CFRP	Carbon Fiber Reinforced Polymer
AFGT	Axial Functional Graded Thickness
LFGT	Lateral Functionally Graded Thickness
FEA/M	Finite Element Analysis/Methods
NIP	Number of Integration Points
FVD	Force Versus Displacement
NTEPF	Near To impact End Progressive Failure
PCF	Peak Crushing Force
IDM	Incomplete Diamond Mode
FM	Failure Mode

ABSTRACT

Shinde, Shantanu R. M.S.M.E., Purdue University, August 2019. Origami Inspired Design of Thin Walled Tubular Structures for Impact Loading. Major Professor: Dr. Andres Tovar.

Thin-walled structures find wide applications in the automotive industry as energy absorption devices. A great deal of research has been conducted to design thin-walled structures, where the main objective is to reduce peak crushing forces and increase energy absorption capacity. With the advancement of computers and mathematics, it has been possible to develop 2D patterns which when folded turn into complex 3D structures. This technology can be used to develop patterns for getting structures with desired properties.

In this study, square origami tubes with folding pattern (Yoshimura pattern) is designed and studied extensively using numerical analysis. An accurate Finite Element Model (FEM) is developed to conduct the numerical analysis. A parametric study was conducted to study the influence of geometric parameters on the mechanical properties like peak crushing force, mean crushing force, load uniformity and maximum intrusion, when subjected to dynamic loading.

The results from this analysis are studied and various conclusions are drawn. It is found that, when the tube is folded with the pattern having specific dimensions, the performance is enhanced significantly, with predictable and stable collapse. It is also found that the stiffness of the module varies with geometrical parameters. With a proper study it is possible to develop origami structures with functionally graded stiffness, the performance of which can be tuned as per requirement, hence, showing promising capabilities as an energy absorption device where progressive collapse from near to end impact end is desired.

1. INTRODUCTION

1.1 Thin Walled Tubular Structures as Energy Absorbing Devices

Automotive impact fatalities occur commonly worldwide. According to a report from the World Health Organization [1], about 1.2 million people died and about 50 million people were injured due to automotive fatalities. From a public health perspective, motor vehicle crashes are the fourth leading cause of death after heart attack, cancer and stroke. Apart from the heavy toll on human lives, impact accidents also cause damage to other structures and environment involved.

The first automotive accident occurred in New York City in the year 1889 [2]. This event led to the inception of the field of automotive safety. Today, occupant safety has become one of the most important design criteria for evaluating the overall performance of a vehicle. Automotive safety improvements over past few decades have focused on crash avoidance technology, structural crashworthiness, and occupant protection devices. Modern vehicle safety technologies along with improved highways, better traffic control and better driver education has contributed to an impressive drop in the fatality rate due to vehicle crashes. The fatality rate in the United States has dropped from 20 in 100 million miles to 1.16 in 100 million miles between 1935 and 2018 [3].

In spite of the continuous drop in the vehicle crash fatality rate, the statistics of traffic injuries and deaths are astonishing. According to a report from IIHS, a total of 37,133 people died in vehicle crashes in 2017 in the U.S [4]. Hence, there is still a need for continuous improvement on both, active and passive safety of a transportation vehicle. Figure 1.1 indicates the number of motor vehicle crash deaths 100,000 people.

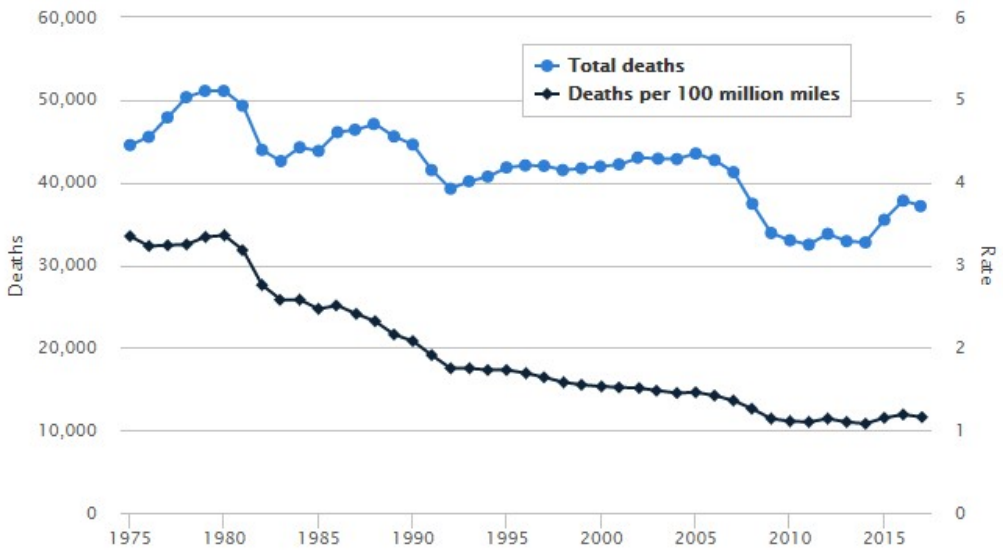

Figure 1.1.: Motor vehicle crash death per 100,000 people by type, 1975-2018 [4]

A most common approach of minimizing the loss of life and property in an impact accident is to install energy absorption devices in the structures, which are designed to convert, totally or partially, kinetic energy into another form of energy during the accident so that damages to the important main structures are mitigated [5]. An ideal energy absorption device should meet the following requirements [6]:

- Irreversible energy conversion to avoid a second impact caused by energy release.
- Long stroke to allow space for plastic deformation
- Stable and repeatable deformation mode to ensure predictable performance in each impact.
- Restricted and constant reactive force so that no excessive force is transmitted to the main structure to be protected.
- Light weight and high energy absorption to absorb as much energy as possible.
- Low cost and easy installation as it is a one-shot device and needs replacement after an impact accident.

Practically, two parameters are extensively applied to evaluate the energy absorption performance of a device: the specific energy absorption (SEA), defined as the energy absorption per unit mass, and the load uniformity, defined as the ratio of the peak force to the mean crushing force [6]. Peak force is the highest reaction force during the crushing process and the mean crushing force is the total energy absorption dividing the final crushing distance. A review of various designs for thin-walled tubular structures as energy absorbing devices is presented in section 2.2 of chapter 2.

1.2 Crashworthiness

1.2.1 Background

The greatest gift to any living being on this planet earth and anywhere in this universe is the gift of life and everything good eventually comes to an end. The end to a life would be death in this case, which comes in a number of forms. Depending on how or with what beliefs a person's upbringing was influenced would define the existence of man, creation or evolution, whichever it may be, a person's demise in the early stages were mostly due to sickness which early man didn't understand or death by tragedy. People learn, cures were made, but death is inevitable.

As humans understood how they could use the environment to their own benefits modes of transport changed from animals to machines which are termed as vehicles today. Vehicles are an important and inseparable part of us now, lots of events depend on it, right from saving a person's life to the economy of a nation. Unfortunately, it has also happened to be the cause of fatality. As per records [7] the first automobile accident took place in Ohio in the year of 1891 where in James William Lambert driving a single-cylinder automobile crashed into a post after his car lost control initially when it hit a tree root which didn't result in any fatality but minor injuries and the first fatality recorded was that of Henry H. Bliss in the year of 1899 in New York when his vehicle was struck by an electric taxicab and succumbed to injuries the

very next day, an event which may have led to Automotive safety as a topic which is intensively researched upon till date. Statistics released by the World Health Organization (WHO) state that on an average there are 3700 deaths per day on the world's road and tens of millions of people are injured or left disabled [2]. Ever since the motorization of the United States of America, 6 times more the number of people drive a vehicle than they did in the 1900's and the number of miles travelled is probably 10 times higher too [2]. From a health-related perspective motor vehicle fatality rank no.4 in the world's leading causes of death. One would say data would show number of deaths increased too, but the death per 100 million miles travelled has dropped from 18 to 1.7 in America, which is almost a 90% decrease. This is solely to the fact that research and development in automotive safety has had a major facelift.

1.2.2 Motor Vehicle Safety

Vehicle design has many aspects and one such design objective that is major factor is vehicle safety. Du Bois P. et al. [2] state that there are three distinct periods or rather three stages which have led to automotive safety to where it is today. Beginning of the new century, manufacturers realised that automotive safety is a topic they should start stressing over. With the tools and innovations available in that time the first period saw the manufacturers starting with basic needs. This period saw the addition of headlamps for better vision in low light, wind shield to protect the occupants from objects flying into them, managing better tyres to reduce tyre blowouts and an all steel body structure to protect its occupants. Apart from the vehicles directly, governments added STOP signs, lane markings, converted streets into one-way streets too. This period also gave the world its first ever full-scale crash test where tests include roll over and barrier impact. Du Bois P. et al. [2] mention that the second period was from 1935 to 1950. This period saw upgrades to the devices updated in the first period, better headlamps, dual windshield wipers, turn

signals and it also saw different types of testing performed. Testing in this stage was unsophisticated, it was basic and results were solely dependent on observations, there were no dummies in the occupant cabinet nor there were electronics to read and record data from crash tests. The world saw its first full frontal crash test simulation where in a vehicle was launched into a retaining wall. The most significant development of that age which the world is thankful for till date is the seat belt.

Up until this period vehicles were would heavy and bulky to reduce harm to cabinet occupants of the said vehicle. The developments so far were basic, the introduction of wiper blades, rear view mirrors, turning indicators, headrest, laminated glass, padded dashboards to name a few. At the turnaround of the 50's and 60's automotive safety saw a boom in advances. 1952 saw Mercedes Benz engineer Bela Barenyi invent the 'crumple-zone' concept, which in a crash event would absorb the impact forces. This concept is an area that is widely researched upon today to the fact that each component of the vehicle frame is designed to absorb forces and maintain the body structure. One other invention that led to a Le-Mans win in 1953 for Jaguar and Dunlop was the invention of disc brakes and in 1959 saw Volvo the use of Nihl Bohiln's three-point seatbelt which is the most effective invention till date. 1960's saw the implementation of safety regulations and the National Highway Safety Administration (NHTSA) was created and during this period many mandatory safety standards, Federal Motor Vehicle Safety Standards (FMVSS), were introduced that regulate aspects of vehicle crashworthiness and crash avoidance performances due to which auto manufacturers had to add in certain features and build the car to perform in a certain way during a crash which has capped the fatality rate per million vehicle miles travelled to 1.7 over time.

From crash performance, manufacturers have gone a step ahead and built in electronic systems that are termed as crash avoidance systems, such as anti-lock brakes, traction control, lane management system, heads up display, cruise control, etc. Considering all the upgrades and inventions in electronic and mechanical systems to make the vehicle stronger, it is important to mention that the biggest improvements have

come in the good old-fashioned steel and body structure of the vehicle. Before going to crashworthiness, it is important to briefly discuss the evolution of materials and structure used.

1.2.3 Materials

The automotive industry has used and is using a tremendous amount of materials to manufacture a car which include and are not limited to, iron, aluminum, steel, glass, rubber, petroleum products, copper, steel, etc. These materials have undergone changes over time and have become sophisticated and better built also safer. Their change is greatly due to the fact of innovation in manufacturing technologies [8].

The most common material used in the industry to manufacture vehicles is steel which allowed for mass production of a million of vehicles economically. The requirements from the material are corrosion resistance, good formability, strength, light weight, controlled deformation under crash and others that depend on the application. The first full steel vehicle body was built by Dodge in 1924. Vehicle bodies have gone from being bulky and heavy and built like a tank to being light weight and energy absorbent, all though the decision comes down finally to the application the vehicle.

Vehicle bodies need not necessarily be made of the same material throughout as manufacturers have been known to implement a number of materials, such as the 2015 Volvo XC90 uses 5 different grades of steel and lightweight aluminum. It might be good to have a body that is heavy and bulky but it doesn't mean safe because running into a stiff wall with a heavy vehicle equipped without proper energy absorption material the vehicle would 'bounce off' [8] and the deceleration would pass through the whole body and the passenger which can be fatal.

When creating a car, its mass is the most important thing as everything is affected by it, right from building an engine that can propel it forward to pollution due to the harmful substances emitted into the atmosphere to the inertia of the car for its

acceleration and braking, it becomes important to spend less energy in doing the above mentioned [2]. One good way to achieve this is via the use optimum materials. By using appropriate material as per the functional requirement, optimal material layout can be achieved. The Figure 1.2 below is a representation of the same.

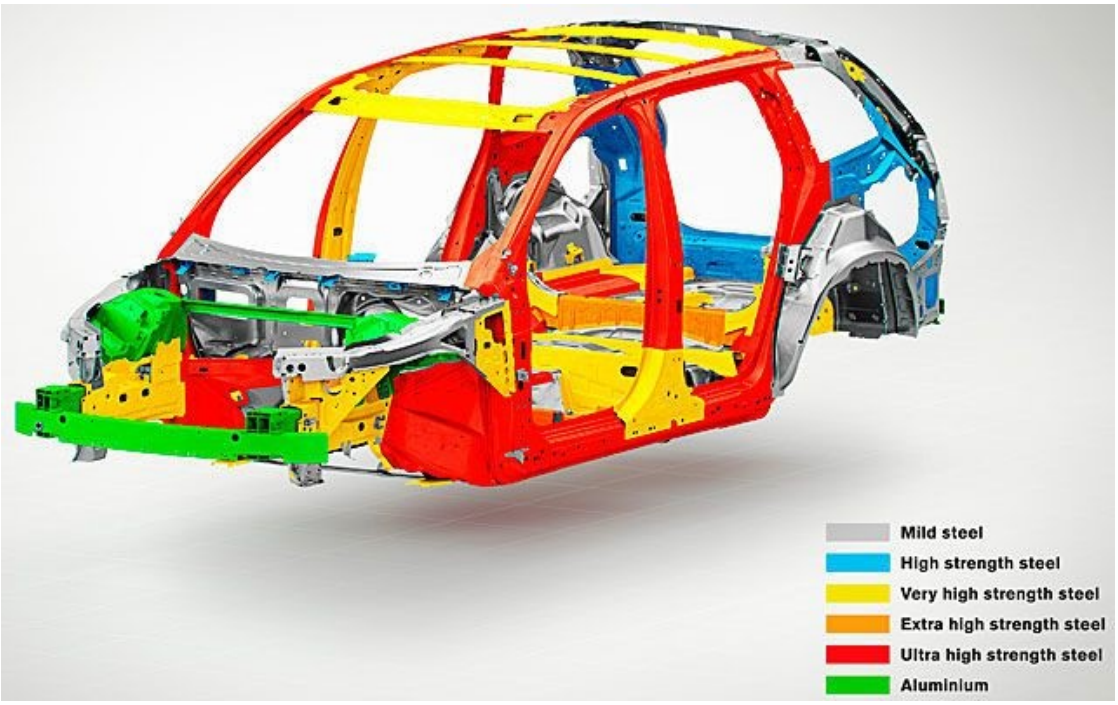

Figure 1.2.: Use of Materials in a Vehicles Structure [8]

More than half the volume in production of a vehicle in the past age consists of cast iron and steel parts, i.e., 55%, 11% is plastic, 9% is aluminum alloys followed by rubber with 7% and the rest.

Composite materials are making their presence felt as modern engines materials use the basis of composite with an aluminum matrix which represents an alloy of aluminum with added fibers of silicon and carbon. The use of polymer materials has known to reduce manufacturing costs [8]. So, one can observe the automotive industry is constantly on the move to satisfy consumer needs of light and safe vehicles by improving manufacturing technology and economy at the same time. Figure 1.3 shows the use of materials in the industry.

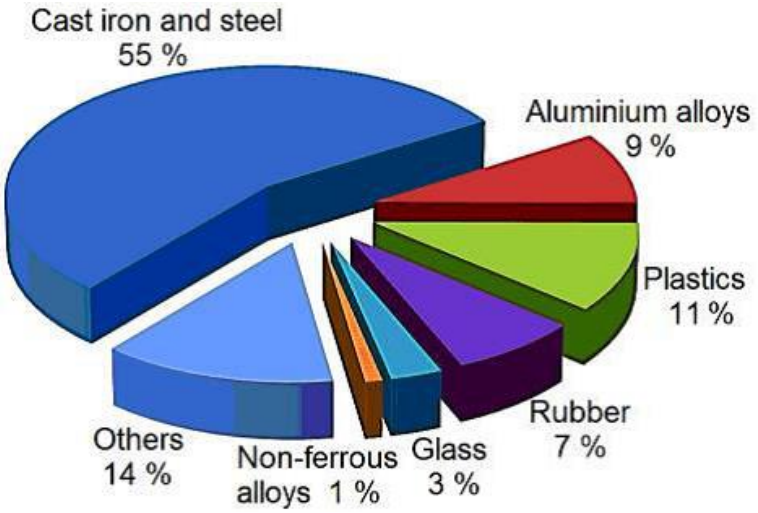

Figure 1.3.: Pie Chart Showing Usage of Materials in the Market [8]

1.2.4 Vehicles Structure

A vehicles structure is designed to withstand static and dynamic loads encountered during its life cycle. The interior and exterior are built to satisfy different requirements such to provide space for the occupant and a shape to provide low drag coefficient respectively [2]. The vehicle body is mounted on suspension to reduce vibration transfer to the occupants. The structure of the automobile has undergone many changes over the decades from being boxy to streamline. At this stage a car body structure can be classified into two categories: body-over-frame structure and unit-body structure.

The body-over-frame structure is simply a body of the vehicle and its chassis manufactured separately and the body mounted on the chassis frame and fastened. Here the body provides the necessary strength in bending and torsion. The frame supports the drive train, suspension and other parts. The vehicle body is not directly attached to the chassis frame but via shock absorbing mounts which reduce high frequency vibrations. An example of such a vehicle as shown below. Mostly used in towing or off-roading vehicles because of the ladder frame chassis resistance to bending.

Figure 1.4.: Body-Over-Frame Structure [2]

Unit-Body Structures, as shown in Figure 1.4, are ones where in the body frame and front sheet metal are one single unit. These are widely used in the modern age. Assembled using spot welding or other fastening methods, this structure is claimed to enhance the integrity of the vehicle, result in weight reduction and better crush performance. Figure 1.5 below depicts such a structure.

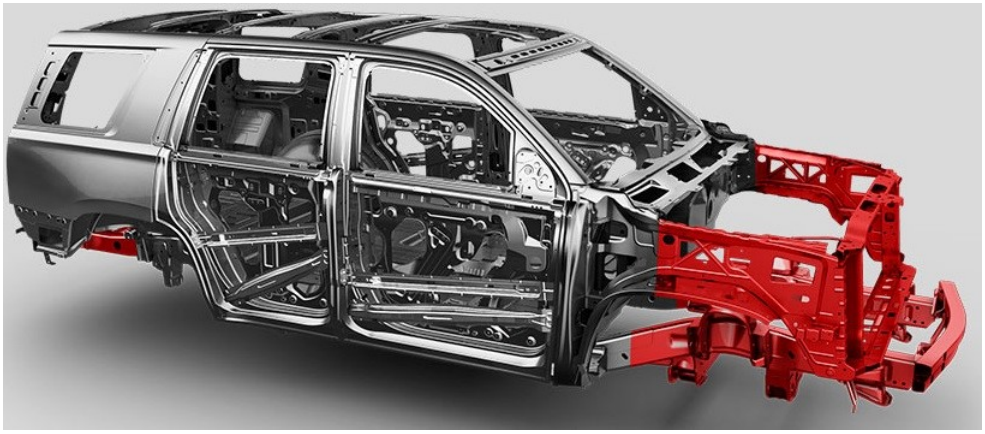

Figure 1.5.: Unit-Body Structure [2]

1.3 Built to Crash

1.3.1 Crashworthiness and it's Goals

The term crashworthiness was first widely used in aerospace industry in the 50's. A term that is defined by Du Bois et. al. [2] as the "measure of the ability of a structure and any of its components to protect the occupants in survivable crashes". It is about safeguarding the occupants of a vehicle to reduce the chances of fatalities. Crashworthiness evaluation is ascertained by a combination of tests and analytical methods [2]. A book published by Ralph Nader in 1964 'Unsafe at any Speed' was controversial to the fact that it pointed out the hazards of some vehicles gaining public attention and the resulting actions add to the drama. The results of an impact study of a structure is always fascinating and reveals a lot. There is a term in crash tests, time zero, it is the time at and after which the violence begins, where the crush zones tell us their story and when everything is said and done, the results say if the vehicle is crashworthy or not.

To compare crashworthiness goals over the years, vehicles in the early stage were made with wood and avoiding deformation were crashworthiness goals. Now, vehicles are made with composites and various materials and also with crush zones, non-intrusion beams, progressively collapsing beams, etc. and now the goal of crashworthiness is to build an optimized vehicle with controlled deformation to absorb the energy during a crash in a way that minimum crash loads are transferred to the vehicle's occupants. Complexity arises with the term 'real-world' collision, where in one could say every crash has its own dynamic events that are unique. So, you could say, crashworthiness is a term that doesn't have a cap on it, it is something that the auto manufacturers have to constantly update when they reconstruct accidents to analyses vehicles crashes which provide them with important data helping them make vehicles much safer, preparing for said event.

1.3.2 Crashworthiness Tests

The world has come far enough to gain data from crash simulations to determine if a vehicle is crashworthy or not, but to date the final assessment for crashworthiness still rely on tests performed in labs which is true during certification of a vehicle [2]. Crashworthiness tests are split into three categories: component tests, sled tests and full-scale barrier impacts which is also in order of complexity with the component being the least complex comparatively with the other two tests and full-scale barrier tests being the most complex. A component test is a test performed to an isolated component to determine its energy absorption capacity and to identify its crush modes.

A sled test makes use of a buck which represents the occupant's compartment with most or all of the components which will be present in the vehicle including dummies [2]. It lets the engineers simulate the dynamic conditions of a full-scale crash event at a fraction of the cost of a crash test. It provides data around which seat belts, steering wheel column, air bags, etc. can be developed. Evaluation of restraints is the primary objective of a sled test [2]. Figure 1.6 shows what a sled test looks like.

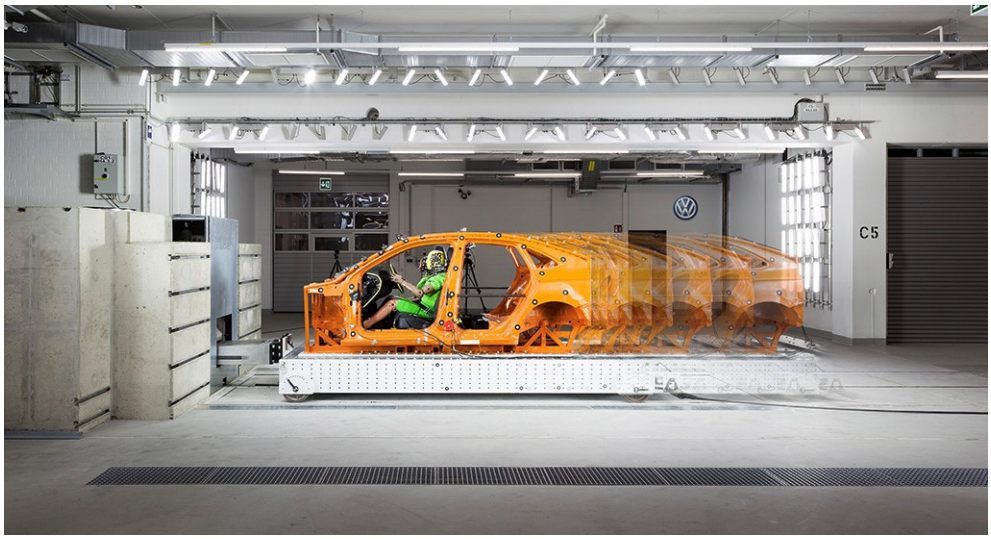

Figure 1.6.: Sled Testing at a Volkswagen Facility Structure [9]

A full-scale barrier test is one where in a guided vehicle is driven into a barrier at speed that is predetermined with initial angle and velocity. A complete vehicle with a dummy passenger is used in such tests. Such tests are performed to ensure that a vehicle is manufactured in compliance with "government-mandated regulations". A dummy performance is evaluated at a speed of 35 mph which is known as the New Car Assessment Program (NCAP) test which allows the engineers to evaluate the restraint systems. Figure 1.7 shows what a Full-Scale barrier test looks like.

Figure 1.7.: Full-Scale Barrier Testing [9]

It is fascinating to note that around 100 prototype vehicles are tested to ensure worthiness and compliance with the International and country specific regulations of a vehicle which can cost a manufacturer around $400'000 - $800,000, which is why manufacturers are pushing for the need to simulate crash event using mathematical models to determine the crashworthiness of a vehicle [2].

1.4 Origami

1.4.1 Introduction

History would say folding and unfolding would be, if not then, one of the most important mechanisms that has ever been come across, the simplest mechanism that can create the most complex mechanism. Also, folding has its own cultural roots in Japan in the name of Origami. Origami is a Japanese art form of folding paper into various shapes and sizes. The word originated from two Japanese words, oru, -ori which means fold and kami which means paper. A paper crane shown below in Figure 1.8 is a famous example of this art form. This segment shall serve as an introduction to Origami.

Figure 1.8.: Origami Crane [10]

Traditional origami was seen practiced during the Japanese Edo period which dates back to 1603. Origami has been present for a long time, but advances in its applications have come in recent times [11]. It has seen its applications in Aerospace, Mechanical, Architecture, Medicine to name a few fields of science. Using the tech-

nique of folding a sheet of paper to something flat and 3D is very fascinating. It is not just an art form anymore it is more than that, it has evolved into a field of study explored in even the farthest spectrum of Engineering.

Usually it could be something random, one would try to find new shapes and at times there is intensive math behind them, using which one would make a crease pattern and to get the desired shape the artist would then fold accordingly. To understand what a crease pattern is, let us dive into some terminology. A crease is a fold. A crease can either be convex or concave, a convex fold is called a mountain and a concave fold is called a valley. Refer Figure 1.9 for better illustration. A crease pattern would than simply be a collection of valleys and mountains [11].

Furthermore, a vertex is a point that serves as an origin for lines or where lines meet and as such a degree of vertex would the number of line that meet/originate from the vertex. The result of folding is known as the folded state. The most common crease patterns in Origami are Miura-Ori, Waterbomb base, Nojima and Yoshimura Tessellations.

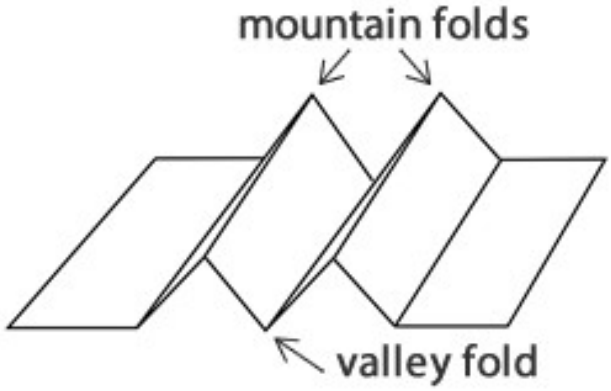

Figure 1.9.: Mountain and Valley folds

1.4.2 Origami Mathematics and Rules

Mathematics has its roots in Origami as well. To start with there are 4 basic rules that a flat-foldable crease pattern needs to follow:

I. Two-Colourability: if a crease pattern is coloured with let's say, grey for polygons facing 'up' and white for the ones facing 'down' the pattern so formed should be such that, two polygons of the same colour shouldn't end up adjacent to each other, as such it should be alternating as illustrated in the Figure 1.10: [12].

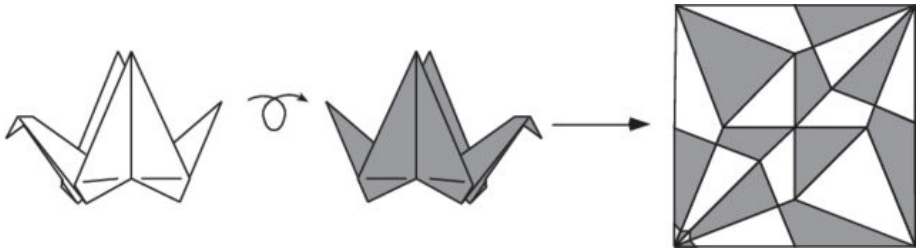

Figure 1.10.: Two-Colourability of a Crane

II. Maekawa-Justin Theorem: the theorem states that the number of mountains and valleys at every vertex differs by two in every direction of flat foldable crease pattern [13], i.e. | M-V | = 2.

III. Kawasaki-Justin Theorem: A flat-foldable crease pattern can be folded flat if and only if at the interior vertex the alternating angles sum up to 180 degrees [14].

IV. No-Self Interactions/Penetrations: this theorem is about no penetrations which states that no face can penetrate another face, no fold can penetrate another fold and no face can penetrate a fold [15].

Apart from the above rules, the Huzita-Hatori axioms are a set of rules that define the single linear folds using line and points. To quote, B. Cipra, et. al. 'these are all of the operations that define a single fold by alignment of combinations of points and finite line segments' [15]. The axioms defined are as follows [12] [16]:

- Given two points p1 and p2, we can fold a line connecting them;
- Given two points p1 and p2, we can fold p1 onto p2;

- Given two lines l1 and l2, we can fold l1 onto l2;
- Given a point p1 and a line l1, we can make a fold perpendicular to l1 passing through the point p1;
- Given two points p1 and p2 and a line l1, we can make a fold that places p1 onto l1 and passes through the point p2;
- Given two points p1 and p2 and two lines l1 and l2, we can make a fold that places p1 onto l1 and places p2 onto l2, and
- Given a point p1 and two lines l1 and l2, we can make a fold perpendicular to l2 that places p1 onto l1. These operations describe simple folds and provide the basic of mathematical origami.

The above laws and axioms are commonly observed in Origami.

1.5 Aim and Scope

Various studies on thin walled tubular structures has shown that there is a strong correlation between the failure mode of the tube and the energy absorbing capability. A conventional tube when subjected to axial loading, requires high crushing force to induce the collapse initially. But when the tube is pre-folded in a such a way that it follows a specific failure mode, the high initial peak crushing forces can be eliminated with no compromise or enhanced energy absorption capacity, given that the tube follows the predefined pattern. The aim of this work is to explore the performance on of thin walled tubular structure with predefined diamond pattern under axial dynamic loading. This work focuses on the structural design and analysis of the tubes by employing numerical approach.As the concepts developed here are purely structural, they can be applied to thin walled tubular structures with different materials and dimensions.

1.6 Thesis Layout

Chapter 2 addresses a brief review of previous research work related to thin walled tubular structures as energy absorption devices. Static and dynamic crushing of square and circular tubes and existing designs of thin walled tubular structure as energy absorbing devices, are emphasised.

Champter 3 addresses the development of a high fidelity Finite Element Model for dynamic axial crushing of the tubes.Various FE modelling elements like the governing and constitutive laws, element formulation, shell properties, material model, contact algorithm, friction model etc used are discussed in detail. A mesh convergence study is performed to find an efficient mesh size. Finally a validation study is done to validate the numerical model.

Chapter 4 discusses the design and numerical analysis of the diamond pattern and focuses on the parametric study of the origami tubes subjected to low velocity axial impact. Subsequently 48 origami tubes having varying configurations are designed and analyzed to investigate the effect of geometric parameters dihedral angle 2θ, l/b ratio (number of modules) and the b/t ratio on the collapse mode and the performance of the tubes. Finally, an approach to design origami tubes with functionally graded stiffness is proposed.

Chapter 5 summerizes the main achievements of the work and suggests potential future work, concluding the thesis.

2. LITERATURE REVIEW

2.1 Axial Crushing of Square and Circular Tubes

Since thin walled tubular structure are widely used as structural members in majority of vehicles, the study of their post-buckling behavior has always been a very important topic of research. The reason for their extensive use is good energy absorption capability, low cost and lower density. They absorb the impacting body's Kinetic energy in the form of plastic deformation, hence safeguarding the passengers and the structure.

A great amount of research has been done on the axial crushing of thin walled tubes which was initiated by Alexander and Pugsley in the 1960s. Various studies uncovered three modes of deformation which were most dominant in axial crushing of thin-walled structures: progressive buckling, dynamic plastic buckling and global buckling (Euler-type buckling). Square and circular tubes are the most used tubular structures as energy absorption devices. Following sections discuss the axial crushing of square and circular tubes in detail.

2.1.1 Square Tube

As already stated, the impact energy absorbed during axial crushing of tube is due to plastic deformations. Hence, the buckling mode has a great significance in determining the energy absorption capacity of a tubular structure when subjected to axial crushing. Various studies [17–20] have reported that there are two main collapse modes for a square tube under axial crushing, i.e. compact mode and non-compact mode. The failure mode depends on the b/t ratio, where b is the width of the square and t is the wall thickness.

Tubes which are substantially thin i.e. ones with high b/t ratio like b/t=100 [21], fail in non- compact mode. Other tubes generally fail in compact mode. Figure 2.1(a) shows the non-compact mode of failure for square tube with high b/t ratio. According to Thornton [17], this mode of failure is undesirable because it may lead to Euler buckling, which reduces the energy absorption capability considerably. Figure 2.1(b) illustrates the compact mode of failure. Depending on the b/t ratio, various collapse pattern like the symmetric mode in which two opposite lobes move inwards and the other two move outwards in the same layer or all four lobes moving inwards or outwards or other asymmetric buckling patterns [18].

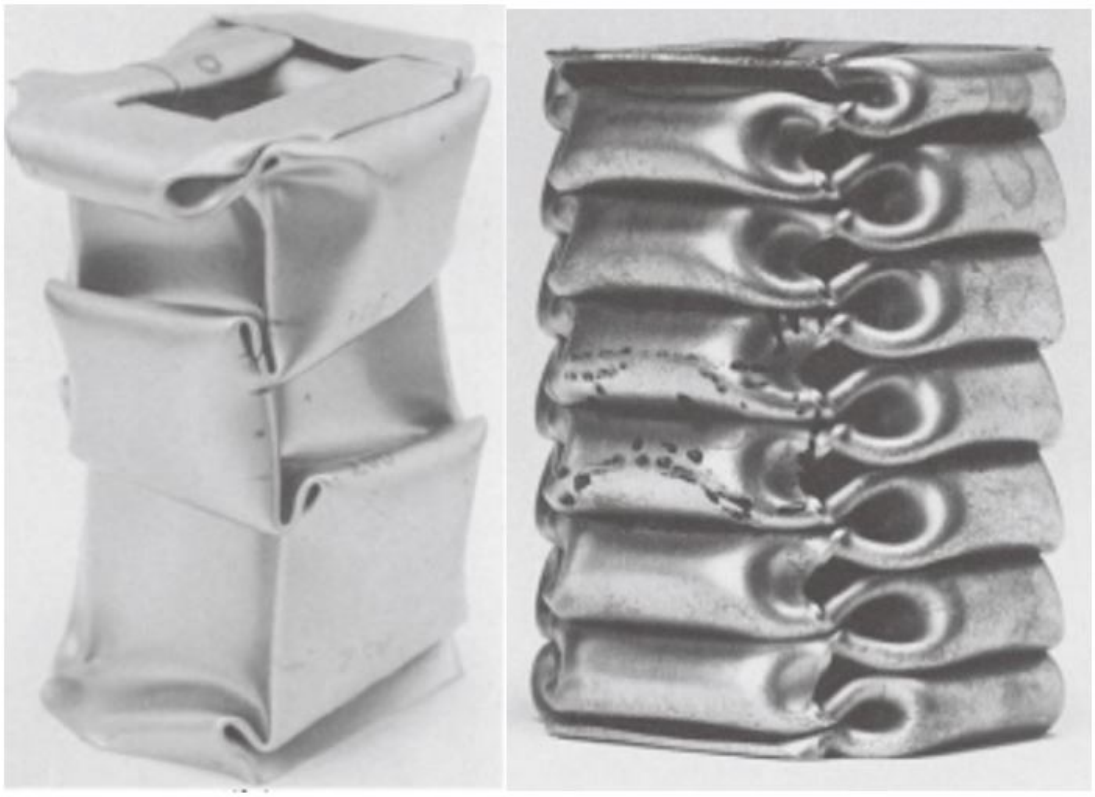

Figure 2.1.: Collapse modes of square tube: (a) non-compact mode and (b) compact mode (symmetric mode) [18]

The tube buckles in a progressive manner, which leads to the fluctuation of crushing force. The first peak load, also known as initial peak crushing force, is evidently higher than the other mountains. This is because very high amount of energy is re-

quired to initiate the buckling of conventional square tube. The force hits the peak crushing force, drops rapidly and then fluctuates periodically. The area below the force vs displacement curve represents the energy absorbed. The mean crushing force is the area under the curve divided by crushing distance. Figure 2.2 shows the force vs displacement curve of a square tube under axial quasi-static crushing.

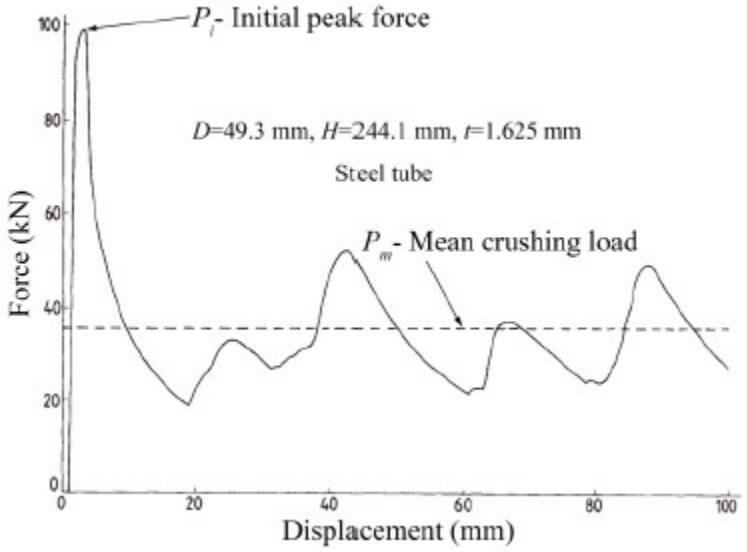

Figure 2.2.: Force vs displacement curve for square tube subjected to axial quasi-static crushing load [18]

Based on the observed pattern of collapse observed in experiments, various simplified theoretical models have been proposed to describe the collapse mechanism of tubes under axial load. Wierzbicki and Abramowicz [22], presented their theory by establishing a basic folding element, also known as super folding element.

It had four trapezoidal elements, a toroidal surface, two horizontal cylindrical surfaces, and two conical inclined surfaces. The energy dissipated by the element came from three main sources, folding along stationary plastic hinge lines, propagation of travelling plastic hinge lines, and localized in-plane stretching in the toroidal surface which was associated with travelling plastic hinge lines. Figure 2.3 shows the super folding element.

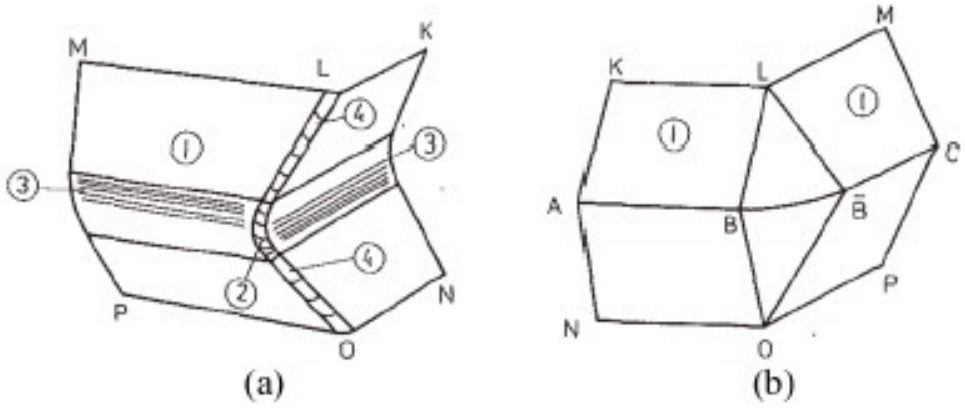

Figure 2.3.: Super folding elements for (a) inextensional folding and (b) extensional folding [22]

The energy dissipated by plastic deformation occurred in the shaded regions. The four trapezoidal elements moved as rigid planes, while the horizontal cylindrical surfaces around the imaginary plastic hinge lines (stationary plastic hinge lines). The propagation of traveling plastic hinges led to the conical surfaces. The localized in-plane stretching occurred in the toroidal surface. Depending on the stated assumptions, they derived a formula to find the mean crushing force for inextentional deformation (compact mode) for square tube having thickness t and width b:

$$P_m = 9.56\sigma_0 t^{\frac{5}{3}} b^{\frac{1}{3}} \tag{2.1}$$

Another important conclusion from this study was that, equal amount of energy was dissipated by the three sources. This indicated that travelling plastic hinge lines account for two-third of the total energy dissipated, making them most effective mechanism for energy dissipation during plastic deformation.

Wierzbicki and Hayduk [18] observed that very thick tubes fail in an extensional mode. Figure 2.3(b) shows a modified model for the theory for accuracy of prediction.

Based on the modified element, Abramowicz and Jones [22] derived the formula to calculate mean crushing force for square tube having thickness t and width b as:

$$P_m = 7.09\sigma_0 t^{\frac{3}{2}} b^{\frac{1}{2}} + 2\sigma_0 t^2 \tag{2.2}$$

A series of experiments conducted by Abramowicz and Jones [[19, 22]] concluded that apart from symmetric mode, the square tube also buckles in asymmetric mode, which is the combination of extensional and inextentional folding element. Two types of asymmetric modes were observed. Figure 2.4(a) shows asymmetric mode A, in which three lobes moved outwards and one lobe inwards and Figure 2.4(b) Symmetric mode B, in which two adjacent lobes moved inwards or outwards.

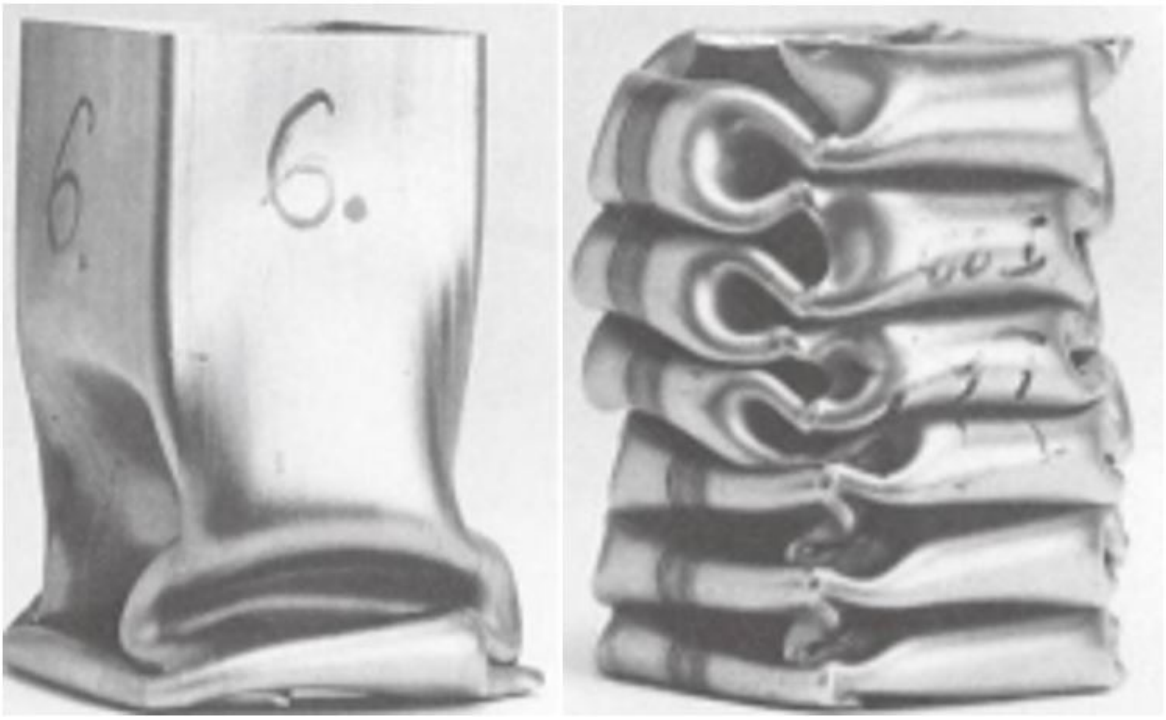

Figure 2.4.: (a) Asymmetric mode A and (b) Asymmetric mode B [22]

Based on super folding element theory and considering the effect of crushing displacement, they derived the formula for mean crushing force as:

Symmetric mode:

$$P_m = 13.06\sigma_0 t^{\frac{5}{3}} b^{\frac{1}{3}} \tag{2.3}$$

Asymmetric mode A:

$$P_m = 10.73\sigma_0 t^{\frac{5}{3}} b^{\frac{1}{3}} + +0.79\sigma_0 t^{\frac{4}{3}} b^{\frac{2}{3}} + 0.51\sigma_0 t^2 \tag{2.4}$$

Asymmetric mode B:

$$P_m = 11.48\sigma_0 t^{\frac{5}{3}} b^{\frac{1}{3}} + 0.44\sigma_0 t^{\frac{4}{3}} b^{\frac{2}{3}} + 0.26\sigma_0 t^2 \tag{2.5}$$

It was also found that in square tubes with b/t>40.8, symmetric mode with inextensional collapse was dominant. Symmetric mode with extensional collapse was dominant in tubes with b/t<7.5. Asymmetric modes A and B were predicted for tubes within the range 7.5<b/t<40.8.

It is evident that the mean crushing force for extensional mode is much higher than the other three modes. Hence, designers always try to design energy absorption devices which will induce inextensional failure mode.

2.1.2 Circular Tube

The collapse modes for the circular tubes are very different than that of square tubes. A circular tube, when axially crushed, collapses mainly in three buckling modes i.e. concertina mode, diamond mode or, mixed mode which is the combination of the two modes.

After performing number of experiments, it was found that buckling mode depends on the geometric dimensions of the tube. Andrew [23] conducted series of quasi-static axial crushing of circular tubes to study the effects of diameter, tube length and wall thickness on buckling mode. A well classified graph was presented in their study. Figure 2.5 illustrates the three major types of collapse modes in circular tube.

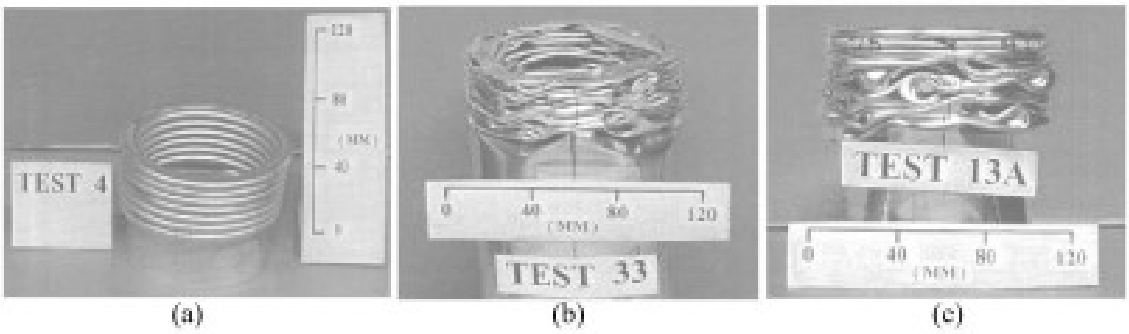

Figure 2.5.: (a) Buckling mode for circular tubes: (a) concertina mode, (b) Diamond mode and (c) mixed mode [22]

Later Guillow [20] investigated the parameters and analytical solutions proposed by Andrew. He provided a well classified chart, as shown in Figure 2.6.

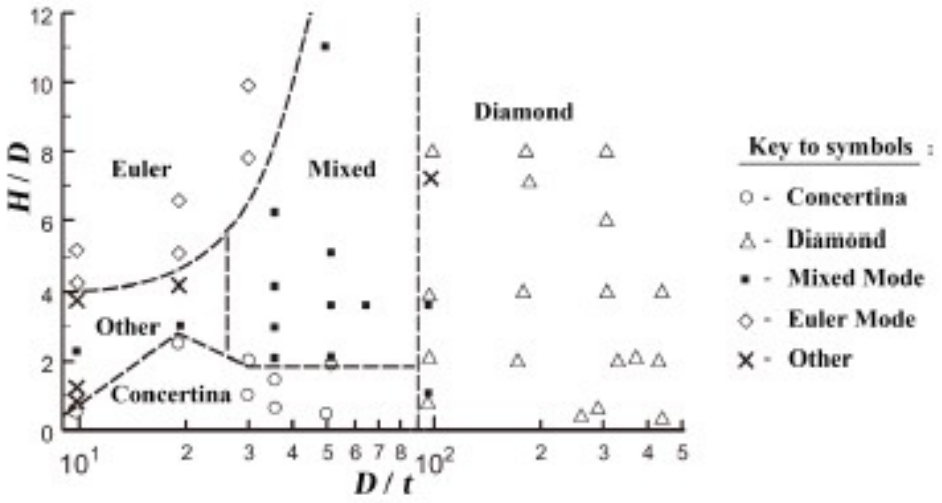

Figure 2.6.: Mode Classification chart for circular aluminium Tube [24]

It demonstrated that that most tubes buckle in diamond mode, when D/t ratio is greater than 90. Concertina mode was observed for D/t<90 and H/D<2. Mixed mode was observed for tubes with 28<D/t<90 and H/D>2. It was also found that slender tubes have the tendency to buckle globally.

2.1.3 Dynamic Effects

All the theoretical analyses reviewed in the previous sections do not consider the dynamics effects. In real world, impact loading occurs, where the energy absorption due to axial crushing takes place dynamically. Dynamic effects due to structure and material complicates the analysis. It is observed that the initial peak crushing forces are considerably higher than the one obtained in quasi-static crushing. This is mainly caused due to inertial resistance and strain rate effects. However, many results from quasi-static analysis can be modified for dynamic analysis by taking the dynamics effects like inertia effects and strain rate effects into consideration.

In low velocity impacts i.e. up to 10 mps, inertia effects are not strong enough, and hence can be neglected. Material strain rate effects which can raise the initial and subsequent yield stress of material, are very significant for strain rate dependent materials and hence should be taken into consideration. The strain rate effects can be taken into consideration by replacing the plastic flow stress σ_{o} in the theoretical analysis under quasi-static loading by dynamic plastic flow stress ${\sigma^{\mathrm{d}}}_{\mathrm{o}}$. The dynamic plastic flow stress can be evaluated using Cowper- Symonds equation, [19, 22, 25]

$$\frac{\sigma_{\frac{d}{o}}}{\sigma_o} = \left(1 + \frac{\dot{\epsilon}}{C}\right)^{\frac{1}{P}} \tag{2.6}$$

Where C and P are material constants and $\dot{\epsilon}$ is the strain rate, which is assumed constant here, even though it varies during impact.

In case of higher impact velocities, like in the case of explosive loading, inertia plays an important role [20]. Dynamic plastic buckling occurs under such conditions. In case of dynamic plastic buckling, wrinkles with small amplitude are simultaneously developed along entire length of the tube when the buckling process begins. In such case, both inertia and strain rate effects should be considered.

In this work, dynamic effects due to strain rate are considered. Since it falls under low velocity impact problem, the inertia effects are negligible and hence not taken into consideration.

2.2 Thin Walled–Tubular Structures as Energy Absorption Devices

Thin-walled tubular structures are the most commonly used energy absorption devices in automotive industry. They can have long strokes, which allows space for plastic deformation. In case of impact, they show stable and repeatable deformation mode, hence ensuring predictable performance. They are cheap, have high manufacturability and are easy to install. All these features make them a good fit for being an energy absorption device. A great deal of research has been conducted to improve the performance of these structures by increasing the EA capacity, lowering the initial peak crushing force, attaining progressive collapse mode, etc. In this section, various types of design proposed for tubular structure as energy absorption devices are discussed.

2.2.1 Square and Circular Tubes with Geometric Imperfections

Square and circular tubes are widely used as EA devices because of their low cost and availability. A great deal of research has been dedicated for improving the performance of these structures. The main objective was to lower the high initial crushing forces required to activate the failure modes yet maintain or enhance energy absorption capability.

Introducing a geometric imperfection was found to be a simple yet effective way for lowering the high initial peak crushing forces. A circular tube with stamped corrugations, Figure 2.7, was studied by Singace and El-Sobky [26] in the year 1997. They found that the high initial peak crushing forces were eliminated and the FVD was more uniform. The only problem with stamping corrugations on tube was that the energy absorbed was substantially lower than that of the similar straight tube.

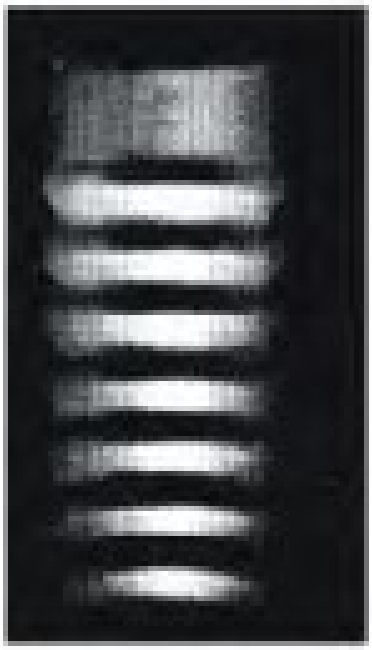

Figure 2.7.: Circular Tube with Corrugations [26]

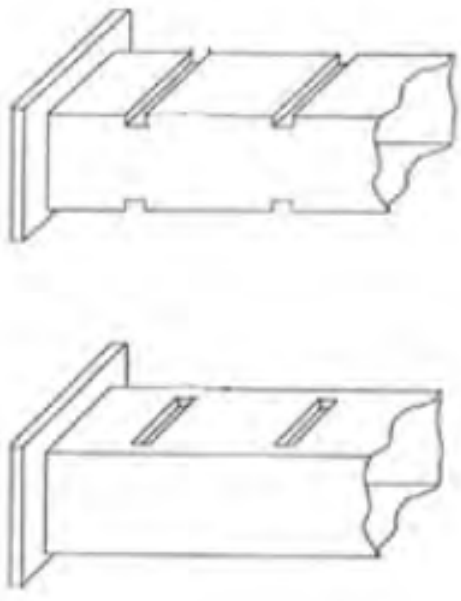

Figure 2.8.: Square Tube with Dents [27]

Dents on the tube, Figure 2.8, were another commonly used type of imperfection. It had similar effect like the corrugated tubes [28–31].

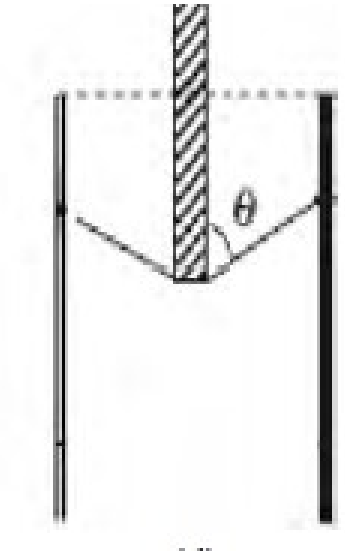

Figure 2.9.: Square Tube with Buckling Intitiators [32]

Zhang [32] overcame the drawbacks of corrugated and dented tubes by designing an innovative buckling initiator, as shown in Figure 2.9, which had a pre-stamped column and pulling strips near the impacting end of the tube.

Various studies focused on increasing the Energy Absorption of the square and circular tubes. Ribs were introduced along the circumference of circular tubes by Adachi [33]. This induced concertina mode in circular tube, the most efficient mode of failure in circular tubes. A 30% of increase in energy absorption was observed from the results from experiments. Lee [27] improved the EA of square tube by 15%- 20% by using controllers. However, the disadvantages like high complexity and high initial buckling forces overweighed the advantages.

Zhang [34] in 2007 made an attempt to achieve both increased energy absorption and low initial crushing force by introducing pre-manufactured pyramid pattern on the surface of square tube. Numerical simulation showed a new failure mode called as octagonal mode, which was similar to the diamond mode in circular tubes. Both low initial peak crushing force and higher energy absorption was achieved when octagonal mode was triggered. Octagonal mode, when successfully triggered, more energy

was absorbed as compared to the symmetric mode typically of conventional square tube and thus making it desirable from the perspective of designing a device for energy absorption. However, experimental results showed that such a mode was very inconsistent.

2.2.2 Polygonal Tubes

Studies have shown that Specific Energy Absorption of circular tube is higher than the square tube with identical dimensions [6]. However, high initial peak crushing forces and inconsistent buckling modes are associated with circular tubes. Hence, tubes with polygonal profile, generally hexagonal or octagonal profile, are used as a trade-of between square and circular tubes.

Abramowicz and Wierzbicki [35] studied the crushing of polygonal tubes and derived an equation to evaluate the mean crushing forces for polygonal tubes. The mean crushing force, for example for a hexagonal tube can be evaluated by equation 2.7.

$$P_m = 20.23\sigma_0 b^{0.4} t^{1.6} \tag{2.7}$$

Mamalis [36, 37] investigated the crushing of octagonal tubes. He observed four modes of failure in the octagonal tube, i.e. extensional mode, inextensional mode, mixed mode and square mode. He found that the energy absorption capacity of octagonal tubes were considerably higher than the identical square tube very close to the identical circular tube.

Yamashita [38] in his work studied the effect of number of sides of a polygonal tube on SEA. He found that SEA increases with number of sides, but stops to increase when number of sides passes eleven. He concluded that polygonal tube with sides greater than eleven acts virtually as a circular tube.

2.2.3 Cellular Tubes

It is known that SEA is directly proportional to b/t. A square tube with smaller width will have higher SEA than the square tube bigger width, given both tubes have same thickness, height and thickness. This is because as the width for square tube increases, its folding wavelength also increases [39]. Hence, the square tube having smaller width will have higher number of folds that the one with bigger width, ultimately leading to higher SEA. This observation was the impetus for the research on multi-cell tubes.

Chen and Wierzbicki [39] studied axial crushing of double and triple cell tubes, as illustrated in Figures 2.10(a) and 2.10(b). They found that the SEA was considerably higher in both case as compared to single-cell square tubes. They postulated a basic folding element and analytically obtained the mean crushing force for both tubes. Kim [41] developed a new multi-cell tube, as shown in Figure 2.10(c).

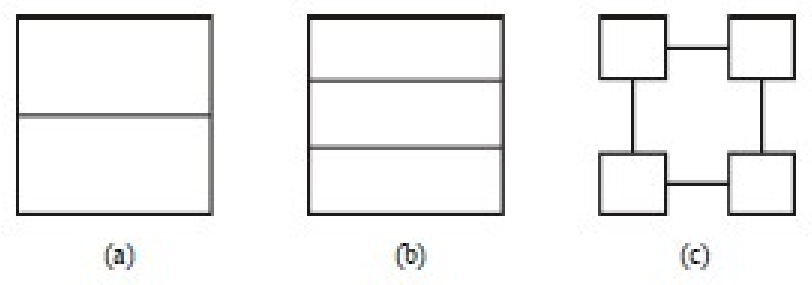

Figure 2.10.: (a)Double-cell (b)Triple cell (c)new Multi cell [40]

It was basically four-square tube connected by plates. It was found that the new design has SEA as much as double compared to conventional square tube. Zhang [40] studied multi-cell square tubes using numerical simulations and theoretical analysis. He concluded that with the increase in number of cells, SEA increases and can be increased 1.5 times by using 3x3 cells.

Though multi-cell tubes had excellent SEA, they are not widely used as energy absorption devices. This is because of complex and costly manufacturing process and high initial crushing forces associated with multi-cell tubes.

2.2.4 Tapered Tubes

Tapered tubes, Figure 2.11, are one of the most used energy absorption devices. They have low initial crushing force, a very stable FVD plot and better performance when subjected to oblique impact compared to straight conventional tubes. Also, sometimes they are used to connect two structural members having different cross-sectional dimensions.

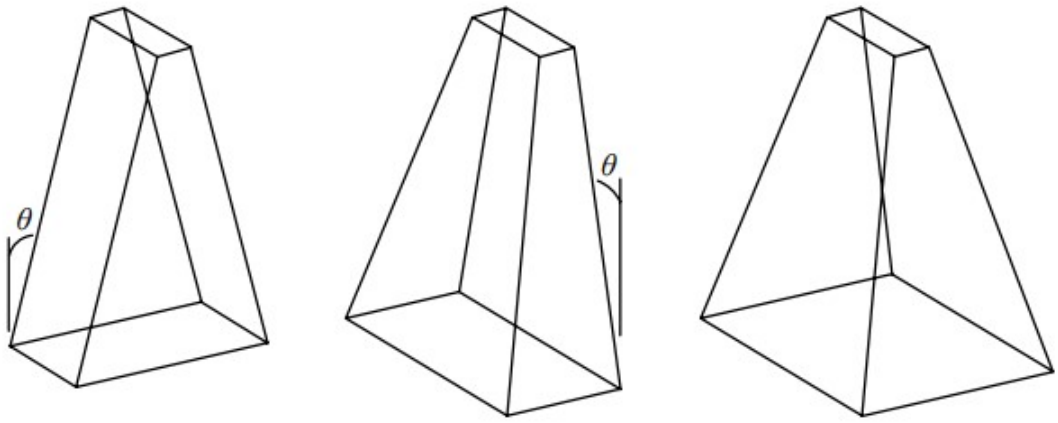

Figure 2.11.: (a) Double taper, (b) Triple taper and (c) Frusta (four tapered sides)

For circular tapered tubes, the failure mode is dependent on geometry of the tube. Mamalis and Johnson [42] studied crushing of truncated circular tapered tube. He found that the tube fails in concertina or diamond mode, similar to the circular tubes. Aljawi and Alghamdi [43] studied the axial crushing of circular tapered tubes with capped frusta. The failure mode observed were outward flattening or inward inversion.

The collapse mode under axial crushing of tapered square tubes is also as same as the conventional square tubes. The tapered square tube collapses in either symmetric mode or extensional mode depending on the geometric parameters [44]. Since the behavior of conventional and tapered tubes are similar, the theoretical analysis for the straight tubes can be slightly modified and applied to evaluate the mean crushing force and energy absorbed by tapered tubes.

2.2.5 Foam Filled Tubes

Filling hollow tube with foam filler has been considered as an effective approach for improving the performance of thin walled tubular structures since a long period of time [45]. The foam fillers reduce the wavelength of the folds, leading to increase in energy absorption. Polyurethane and meatal foams are the most commonly used foam fillers.

Initially much research focused metallic tubes with polyurethane foam [45]. Recently, the combination aluminum foam and honeycomb structure has grabbed attention of researchers due to its promising performance as an energy absorption device. Considerable research [45–50] has demonstrated the advantages of foam filled tubes.

Though foam filled tubes have high SEA, it is not extensively used for the following reasons:

- The effective crushing distance reduces due to foam filling. This is illustrated in Figure 2.12.
- Rupture of the tube under some circumstances, which is undesirable. The cost is relatively high.

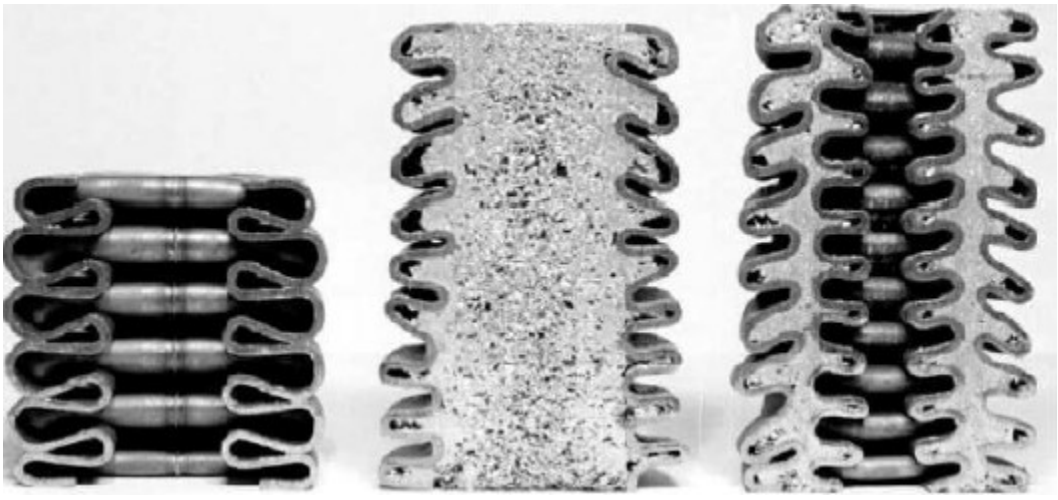

Figure 2.12.: Conventional tube vs Foam filled square [48]

2.2.6 Composite Tubes

In recent time, lot of research was conducted in advancement of composite materials. Its excellent weight to strength ratio makes it an attractive choice in automotive applications. Studies also show that composite material tubes show much higher SEA as compared to metallic tubes.

The most commonly used materials for designing composite tubes are fiber/resin composites. Some examples are fiberglass tubes [62], fiber reinforced tubes [51] and carbon fiber reinforced polymer (CFRP) tubes [52]. It was found that SEA was increased by as much as twice of that of metallic tubes. However, in most cases, these tubes failed in a brittle manner and the failure mode was unstable due to extensive micro-crack development. These factors made them undesirable as energy absorption devices. The brittle failure of CFRP tubes is illustrated in Figure 2.13.

Figure 2.13.: Crushing of CFRP tube

These drawbacks were overcome by using externally fiber-reinforced metallic tubes. This combined the advantages of stable and progressive failure mode of metal and light weight of composites. Numerous studies were conducted metallic tubes with externally bonded glass fiber [53]. The axial crushing showed progressive collapse in these tubes, Figure 2.14, with EA gain of about 50%.

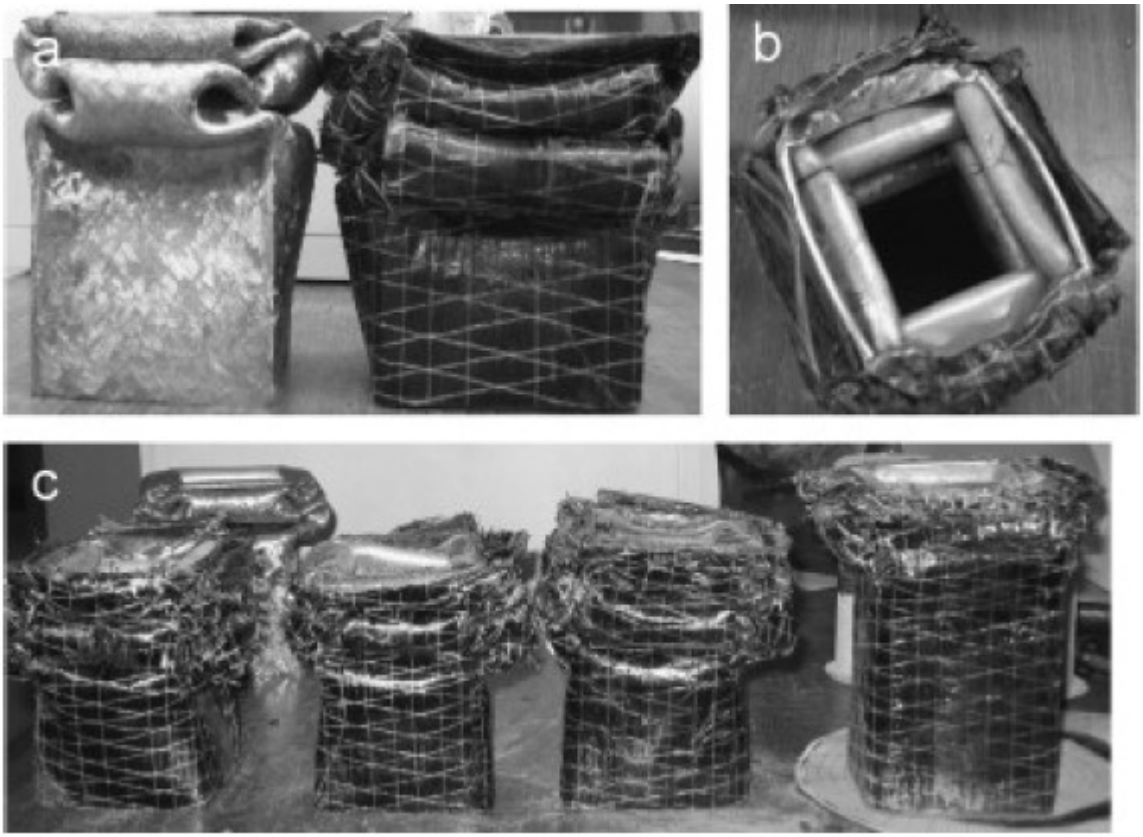

Figure 2.14.: Crushing of externally fiber-reinforced metallic tube [53]

The only drawback of these tubes was that debonding and material fracture were observed for low ductility metallic tubes under dynamic loading.

Sandwich tubes, in which two thin and stiff fiberglass facing sandwich a lightweight polymer foam core in between, are another type of composite tubes. To avoid debonding, local reinforcements are applied to connect facings and the core [54]. This avoids catastrophic failure due to immediate loss of load-bearing capacity due to debonding.

The drawbacks of composite tubes as energy absorption devices is that they are very costly and hence can find application in areas like aerospace engineering and race car design. Also, more research is required to deal with the inconsistent response under various dynamic loading conditions.

2.2.7 Tubes with Variable Stiffness

Another method to increase the energy absorption as well as reducing the peak crushing forces simultaneously, is by proper distribution of tube thickness. Sun [55] in his work, varied the thickness of the wall in longitudinal and circumferential direction, which led to axial functional graded thickness (AFGT), as shown in Figure 2.15, and lateral functionally graded thickness (LFGT), as shown in Figure 2.16.

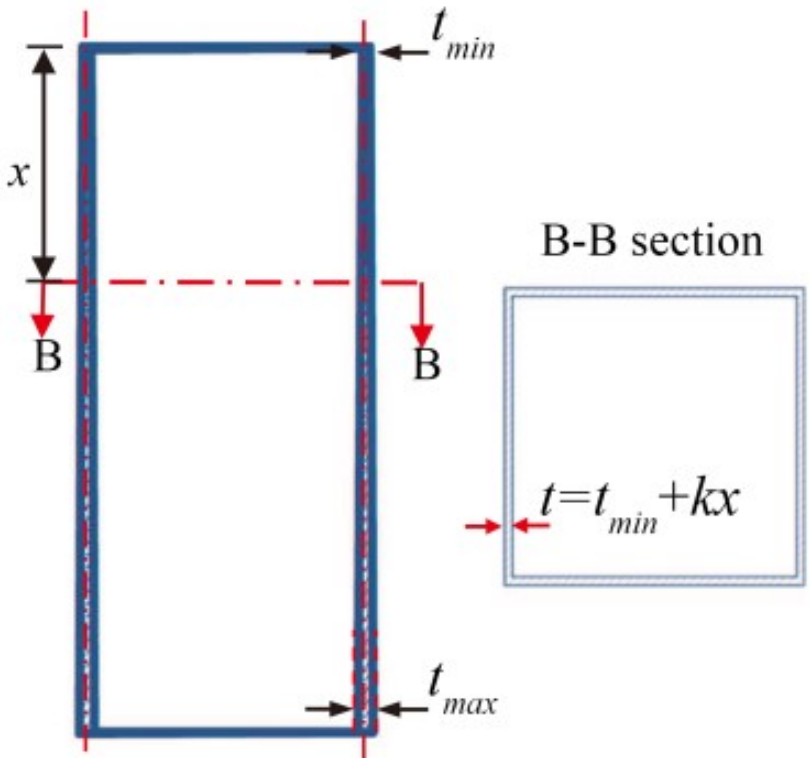

Figure 2.15.: AFGT square tube (sectional view) [55]

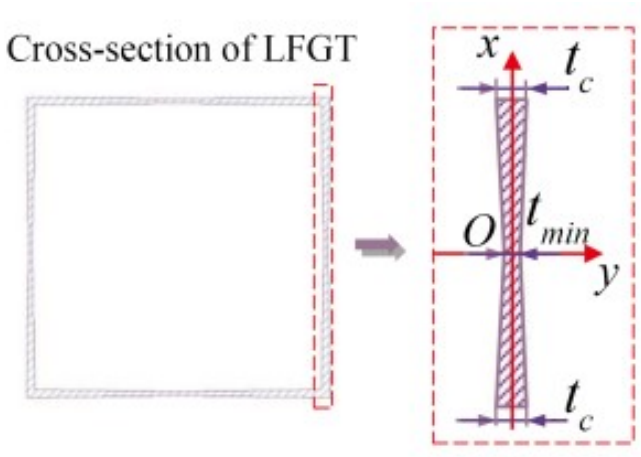

Figure 2.16.: LFGT square tube (sectional view) [55]

He studied these tubes theoretically, experimentally and numerically under uniaxial quasi-static load and found that AFGT square tubes have low peak crushing forces compare to identical uniform thickness tubes and LFGT are associated with increased energy absorption.

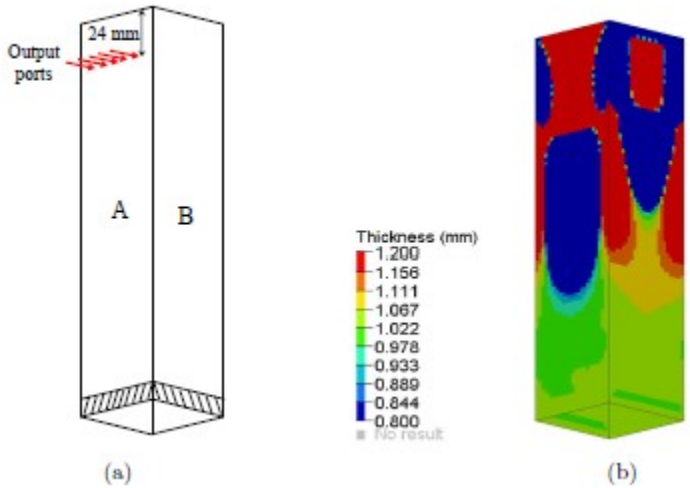

Figure 2.17.: (a) output port location and (b) thickness distribution for the designed tube [56]

Another method was introduced by Bandi and Tovar [56], where they used a design methodology based on topometry optimization for compliant mechanism design

to design thin walled tubular structure for progressive collapse under axial oblique impact loading. In this methodology, the location and direction of output ports, as shown in Figure 2.17, determined the collapse mode. The designed tube was able to initiate a specific failure mode from near to impact end of the tube, stabilize the collapse and reduce the peak crushing forces.

2.2.8 Origami Tubes

An ideal energy absorbing device is one which has high energy absorption capacity, low initial crushing force and low cost. From the literature study up to this point, it is evident that none of the design approaches have the advantage of all three qualities.

The conjunction of Engineering and the art of origami was able to solve this problem. With the advancement of computers and mathematics, it is possible to develop 2D patterns which when folded turn into complex 3D structures. This technology can used to develop patterns for getting structures with desired properties.

Using this approach, a thin walled tubular structure can be pre-folded using a proper origami pattern in such a way that it buckles in a pre-defined, efficient buckling mode, high energy absorption and low peak crushing forces can be attained. In recent years, this approach is gaining great popularity.

Song and Yan [57] introduced various origami patterns for thin walled tubular structures. They studied these structures under axial crushing using numerical and experimental approach. They established the critical states where the crushing mode follows the initial pattern. The developed an equation which gives the relation between mean crushing force and geometric parameters.

Ma [58] in his work proposed a novel origami pattern, which has the ability to trigger diamond mode. He performed extensive numerical analysis to study the crushing of the tube under quasi-static axial crushing. He establishes a basic element for the origami tube, similar to super folding element. His design achieved increase in mean crushing force by 70% and lowered peak crushing force by 25%. He also proposed a

kite shaped origami design [59] in which he was able to lower the peak crushing force by 30% and at the same time increased the mean crushing force by 57%. In his work, he also developed a cost-effective manufacturing process for the origami tubes.

2.3 Summary

The application of Origami Engineering in the area of crashworthiness has just begun to unfold. Researchers are showing their interest in exploring this new field. Most of the investigation until now are performed under quasi-static loading condition to establish the basic theoretical basis for folding element. But, in real life, crashworthy structures are subjected to dynamic loading. For example, the automotive crash-box is design to withstand a low velocity impact, whereas the S-rail is designed for high velocity impacts. The response of thin-walled structures under dynamic loads is different due to introduction of inertia and strain-rate effects. This work focuses on the study of thin-walled tubular structures with pre-defined origami diamond on it, subjected to a low velocity impact loading. The effect of geometric parameters of the pattern on the performance parameters are extensively studied. Finally, a method for designing a thin-walled origami structure with functionally graded stiffness is proposed.

3. NONLINEAR FINITE ELEMENT MODELLING OF THIN-WALLED TUBULAR STRUCTURE UNDER DYNAMIC LOADING

The collapse of thin-walled tubular structure is a very complex problem having multiple physical interactions. The main contributors to its complexity are rate dependence of material, complex material failure behavior, instability during buckling process in thin walled structures, contact of wall and impactor, self-contact between lobes, boundary and initial conditions and geometrical properties. It is very important for the analyst to have an understanding of the basic concepts of Nonlinear FEA. Without this it is just a black box which gives output for defined input. Without a good understanding of the basics, the analyst is at great disadvantage, since the simulation results might be misleading for the design process or research.

The objective of this chapter is to review the main theoretical features of non-linear Finite Element Analysis that are applicable to the analysis of crushing of thin-walled tubular structures under impact loading.

3.1 Finite Element Methods

FEM is a numerical method which solves differential equations that represents engineering problems. Initially, FEM was developed for solving structural mechanics problems, but later extended to various other fields of solid mechanics as well as fluid dynamics, heat transfer, and electromagnetism. Nonlinear FEA has gained immense popularity and has become a vital part of computer-aided design. It has contributed a lot in cutting down the design cycle by replacing numerous testing of prototypes by nonlinear FEM simulations, which provides more rapid and less expensive way to

evaluate design concepts [60]. In Automotive design, the full-scale tests are replaced by crash simulations to evaluate both initial design concept and final design. It has speeded up the design process in the field of manufacturing by simulating processes like sheet-metal forming, casting etc. Drop tests are replaced by simulations for evaluating the durability of the product in electronic industries.

FEM's roots can be found in Euler's work in the 1500's. However, the first mathematical paper was written by Shellback and Courant [61]. It was bought into practice to solve practical problems in structural mechanics in the aerospace industry in 1950's [61].

The finite element formulation is a set of PDE's with a set of initial and boundary conditions, which define the system. These are obtained by applying fundamental laws of nature of the system. The entire system is subdivided into finite number of sub-systems, called finite elements. Each finite element represents a simpler set of algebraic equations. These simpler equations are then assembled into a larger system of equations that models the entire system. These equations are then solved using various numerical methods. The approximate solution is then obtained by minimizing the associated error function using variational methods. There are various types of finite element methods like AEM, generalized finite element method, Mixed finite element method, hp-FEM, hpk-FEM, XFEM, Scaled boundary finite element method (SBFEM), S-FEM, Spectral element method, Meshfree methods, Discontinuous Galerkin methods, Finite element limit analysis, Stretched grid method and Loubignac iteration [61].

3.2 Boundary Value Problem in Structural Mechanics

The crushing of thin walled tubular structure is a boundary value problem Boundary value problem, in mathematics, is a differential equation with additional constraints, known as boundary conditions [61]. The solution to the differential equations must also satisfy these boundary conditions. In structural mechanics, to solve

these problems, the knowledge of structural model, material properties, behavior, the loading and boundary conditions is required. To transform the physical system to a properly defined mathematical model, coherent assumptions and simplifications are needed to get the PDE's that govern the behavior of the structure. The numerical approximations used to solve the PDE's in FEA can lead to numerical errors. By using accurate element formulation, using a refined mesh, scaling the time step, some of these errors can be minimized. But the problem is that it increases the simulation time. Hence, to check and verify the results, a sensitivity analysis for mesh size and time step is done to find a trade of between accuracy and computation cost.

The kinetic and kinematic relationships, thermodynamic laws and constitutive equations required to solve the crushing of thin-walled tubular structure, are summarized below.

1. Kinematics:

   This comprises the deformation gradient and the relationship between displacement and strain.

$$E = \frac{1}{2}(F^T F - I) \tag{3.1}$$

   Where F is the deformation gradient and I is a second rank identity tensor.

2. Balance laws:

   According to the mass conservation law, the mass in a closed system remains constant for Lagrangian formulation [61]

$$\rho_0 = detF\rho \tag{3.2}$$

   Where ρ_o is the density in reference configuration and ρ density in current configuration.

3. Thermodynamic principles:

   Since the process of crushing of thin walled tubes is assumed to be isothermal adiabatic, the heat equation is ignored. The first law of thermodynamics in current configuration is written as [61]

$$\rho\dot{e} = \sigma^T(gradv) \tag{3.3}$$

   Where $\dot{e}$ is the rate of internal energy. Due to the above assumption, the second law of thermodynamics is written as [61]

$$-\rho\dot{\psi} + \sigma L \geq 0 \tag{3.4}$$

   Where ψ is the free energy available for work.

4. Constitutive equations:

   The constitutive model is described below:

$$\sigma = E(\epsilon - \epsilon_p) \tag{3.5}$$

$$f(\sigma, \alpha) = |\sigma| - |\sigma_\gamma + K_\alpha| \tag{3.6}$$

$$\dot{\epsilon_p} = \gamma sign(\sigma) \tag{3.7}$$

$$\dot{\alpha} = \gamma \tag{3.8}$$

$$\frac{\sigma_{\frac{d}{o}}}{\sigma_o} = \left(1 + \frac{\dot{\epsilon}}{C}\right)^{\frac{1}{P}} \tag{3.9}$$

Where equation 3.5 describes the stress-strain relation for the elastic zone, equation 3.6 shows yield surface, equation 3.7 and equation 3.8 represents the flow law and equation 3.9 is the Cowper-Symonds strain rate relation.

A single governing equation is obtained by substituting the above equations in momentum equation. FEM cannot discretize the moment equation directly. For the discretization of the moment equation, a weak form is required. The principle of virtual work or virtual displacement is used as basis of FEA in displacement based analysis for solids [61]. Since most problems use Lagrangian mesh in solid mechanics, the momentum equation, equation 3.10, due to discretization is written as:

$$M\ddot{u} = f^{ext} - f^{int} \tag{3.10}$$

The most famous method for solving such problems is by using explicit time integration method [61].

3.3 Explicit Solver

The type of integration method used depends on the type of PDE, the response of interest and smoothness of data. For parabolic PDEs, implicit methods are generally preferred [61]. In case of buckling of thin walled structures, the equations for shell elements are parabolic [61]. However, explicit method is used since they are efficient when dealing with contact-impact problem.

3.4 Finite Element Formulation for Thin Walled Tubular Structure under Dynamic Loading

In the case of dynamic crushing of thin walled structure, the kinetic energy of the impacting body is converted to strain energy by plastic deformations in the structure. A large amount of force is subjected in a very small period of time, which leads to nonlinearities. It is necessary to take these nonlinearities into account to get accurate

results, which makes such problems very complex. It is impossible to solve such complex problems using an analytical method, hence numerical methods are used to solve these problems. LS-Dyna, Radioss, Pam-Crash, Abaqus, etc. are the various nonlinear transient dynamic FEA packages that uses explicit time integration. For this study, LS-Dyna was used to simulate the crushing of the thin walled structures. CAD models were modeled using PTC Creo Parametric 3.0 and were meshed using Hypermesh. These mesh models were later imported to LSPP for completing the FE modeling.

3.4.1 Material Properties

Mild Steel was selected as the material, since it is the most common material used for thin-walled tubular energy absorbing devices in automotive industry.

The mechanical properties are listed in Table 3.1, which were taken from [56].

Table 3.1.: Material Properties

Property	Value
Density	7800 kg/m^3
Elastic Modulus	207 GPa
Poisson's Ratio	0.29
Yield Stress	253 MPa
Effective Plastic Strain	Effective stress (MPa)
0.000	253
0.048	367
0.108	420
0.148	442
0.208	468
0.407	524
0.607	561
0.987	608

To model the material in LSPP, Material model 24 MAT_PIECEWISE_LINEAR _PLASTICITY was used, in which an elasto-plastic material with an arbitrary stress vs strain curve and strain rate dependency can be defined [62].

It is based on the Cowper Symonds model. The dynamic plastic flow stress can be evaluated using Cowper- Symonds equation, [19,22,25] expressed as $\frac{\sigma_{\frac{d}{o}}}{\sigma_o} = \left(1 + \frac{\dot{\epsilon}}{C}\right)^{\frac{1}{P}}$.

Where C and P are material constants and $\dot{\epsilon}$ is the strain rate, which is assumed constant here, even though it varies during impact.

3.4.2 Shell Properties

From the literature study, it was found that most of the investigators used shell elements to model thin-walled tubular structures. Experimental results show good agreement with results from shell-based FEA. Due to this reason, 90% of the car model is made up using shell formulation [63]. Generally, thin walled structures are modelled using plane stress shell elements [63]. Various shell elements available in LS-Dyna are listed in Figure 3.1.

LS-DYNA Element Formulation	Name	Properties
EF1	*Hughes-Liu*	Degeneration of 8-node brick, incrementally objective, uniformly reduced integration, nonplanar geometry, one point quadrature
EF2	*Belytschko-Tsay (Lin)*	Computationally efficient, 5 through-the-thickness integration points, co-rotational coordinates and rate of deformation formulation, hourglass viscosity, nonplanar geometry, Hughes-Liu mass matrix
EF6	S/R Hughes-Liu	Selectively reduced integration near boundary and point loads to prevent hourglass, nonplanar geometry
EF7	*S/R co-rotational Hughes-Liu*	Similar to EF6 using co-rotational coordinate system from Belytschko-Tsay
EF8	*Belytschko-Leviathan*	Modified Belytschko-Tsay for passing the patch test, physical hourglass control
EF10	*Belytschko-Wong-Chiang*	Perfectly planar geometry
EF11	*LS-DYNA*	Fast co-rotational Hughes-Liu (EF1)
EF16	*LS-DYNA*	Fully integrated shell

Figure 3.1.: Shell element [64]

Belytschoko-Tsay formulation is used widely by investigators in the study of thin walled structures because it is efficient, uses a reduced integration scheme and is the most robust formulation when large information is required [63]. The Hughes- Liu is subjected to hourglass mode and has one in-plane integration point. This type of formulation is used when there is very large in-plane shearing deformation [63]. The fully integration formulation are the most accurate ones, but most expensive and time consuming due to four in-plane integration points.

Fully integrated shell element (type 16) is used when accuracy is a concern, especially when studying the behavior of structures. The initial element shape is reasonable and element does not distort unreasonably during deformation. Strain rate interpolation is assumed, which alleviates locking and enhances in-plane bending behavior [63]. In problems having finite thickness strain and contact and surface loads, for example sheet metal forming, fully integrated shell with thickness stretch (type 26) is used [63].

Membrane element formulation are also available, of which one is fully integrated Belytchko-Tsay membrane. This element formulation finds application in modeling of airbag, seatbelt, fabric armors, etc. [63].

For this work, fully integrated shell element (type 16) is used to model the tubular structures. It is not subjected to hourglassing because it has 4 in-plane integration points, which ensure solution accuracy. This element is fully integrated shell with assumed strain interpolations used to alleviate locking and enhance in-plane bending behavior [63].

3.4.3 Contact Algorithm

Other than nonlinearities due to deformation, material and strain, contact serves one of the most important nonlinearities in boundary value problem. In the axial collapse of thin walled tubular structure, there are two main contacts, one between the impactor and the tube and other between two adjacent lobes of tube. Contact

interface is represented by motion constraint equation. There are four methods to define contact: Lagrange multiplier, penalty function method, augmented Lagrangian and perturbed Lagrangian method. Penalty function method is used by LS-Dyna as their default contact formulation because it is easy to implement. The penalty function method uses an additional penalty term in the energy equation [65].

Consider a simple mass-spring system as shown in Figure 3.2. The energy equation is expressed as

$$\prod(u) = \frac{1}{2}Ku^2 - mgu + \frac{1}{2}\varepsilon(c(u))^2 \tag{3.11}$$

Where K is the stiffness, m is the mass, u is the translational deformation, g is the acceleration due to gravity, ϵ is the penalty stiffness parameter and c(u) is the constraint equation.

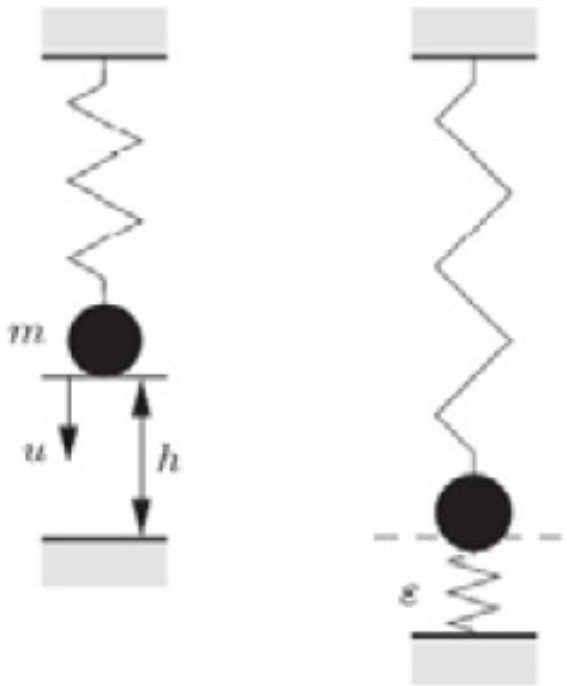

Figure 3.2.: Point mass supported by a spring and a penalty spring due to the penalty term [65]

The contact is treated as an active constraint by the additional energy term. It is nothing but the strain energy of the imaginary spring connecting the two contact boundaries. This penalty parameter is defined as the stiffness of the rigid wall in LS-Dyna [66]. In contact calculations, it is not possible to express the key condition of impenetrability using simple equations. It is expressed in rate form in explicit solvers [61]. In case of a rigid wall striking a tube, the contact force is an important response for the analysis. The contact force for the system shown in figure 3.2 is evaluated by the equation:

$$R_N = \varepsilon(c(u)) = \frac{\epsilon}{\epsilon + K}(Kh - mg) \tag{3.12}$$

Where h is the initial distance between contacting boundaries.

Since the stiffness of the rigid wall is higher than the stiffness of the spring, the penalty stiffness parameter the condition $\epsilon \to \infty$, the contact force is independent of the penalty stiffness parameter. Hence, the contact force is evaluated accurately. The condition of impenetrability between adjacent fold is another key feature of contact algorithm. A single surface is defined to implement this feature.

3.4.4 Number of Through Shell Thickness Integration Points

In the elastic zone, stress varies linearly with respect to thickness, hence the outputs can be easily evaluated by performing integration. But that's not the case in plastic zone. The stress distribution is not linear through the thickness, as shown in Figure 3.3. To account to this nonlinearity, at least 3 through thickness points are required. Higher the NIP, more accurate the results will be, but at the same time computationally expensive. Since internal energy is an important factor in crashworthiness, optimal NIP is crucial.

Studies of behavior of thin walled structure under axial loading have indicated that 5 NIP yield accurate results [56]. In this study, 5 through shell thickness integration points are used.

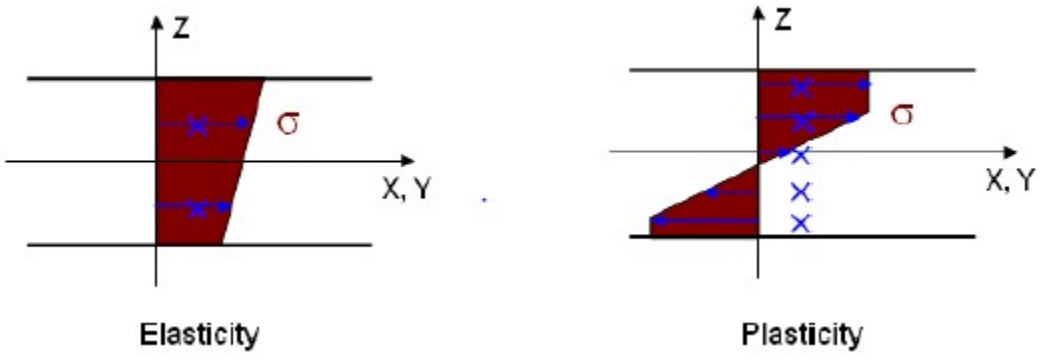

Figure 3.3.: Integration through thickness [61]

3.4.5 Friction

Friction has a great significance in impact simulations. Deviation of friction values from actual values can lead to misleading results. In LS-DYNA, friction is most commonly defined by using *CONTACT card [62]. The relation between coefficient of friction and relative sliding velocity is

$$\mu = F_D + (F_S - F_D)e^{-(DC|\nu_r e|)} \tag{3.13}$$

Where, F_D, F_S and DC are mathematical parameters that modulate the coefficients of friction [67].

Figure 3.4 depicts the relation between and vre with various contact pressure and DC values.

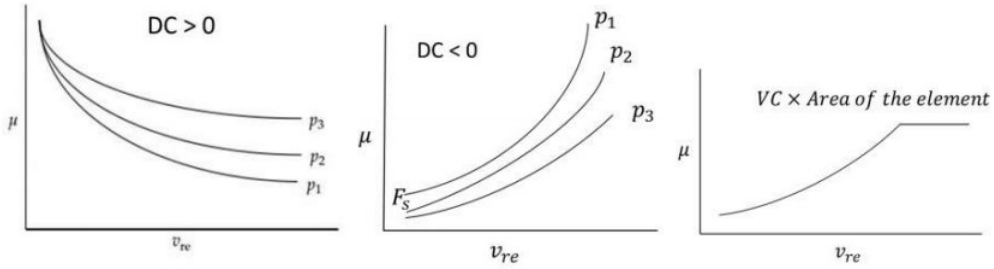

Figure 3.4.: Curve of friction coefficient and relative velocity defined in LS-DYNA [62]

For *RIGIDWALL elements, the friction coefficient is defined separately. Instead of defining a curve, this element only allows to define a constant value for friction coefficient [62].

In this study, Coulomb friction of 0.1 was taken for self-contact of lobes. The contact between the rigid wall and the tube was taken as 0.3 to allow sliding movement [67].

3.4.6 Time Step

Time step increment is very important factor for computational stability of a crash simulation, and must be less than the highest frequency of the system [62]. It is the minimum time required for the crash pulse to pass through the smallest element in the deforming structure. The time step increment is calculated using the formula:

$$\Delta t = 0.9 \frac{l}{\sqrt{\frac{E}{\rho}}} \tag{3.14}$$

Where l is the critical length of the element, E is the Young's modulus and ρ is the density of material.

LS-Dyna has default time step scaling factor as 0.9.

3.5 Mesh Convergence Study

In Finite Element Analysis, it is important to know if the output results are converging, and also if they are converging to an acceptable level of accuracy. In order to assure this, a proper mesh is used in terms of shape and size of the elements. A model with coarse mesh will take less time for the computation, but will hamper the accuracy. On the other hand, a model with fine mesh will yield accurate results on cost of higher computational time. Hence, it is utmost important to have a proper balance between the accuracy and the computation cost.

A mesh convergence study was performed for three mesh sizes, 1.5mm, 2mm and 3mm. To find an appropriate mesh size, the peak crushing force, mean crushing force, Energy and lobe formation pattern were studied. Mean crushing force is calculated as:

$$P_m = \frac{\int_0^{\delta} P(x)dx}{\delta} \tag{3.15}$$

Where, δ is the crushing distance. As stated earlier, LS-DYNA, which is an advanced explicit nonlinear FE code, is used to perform axial crushing under dynamic loading. A square tube which is 240mm long and 60mm wide, meshed with a four-node shell element formulation, as explained in 3.3.2, is considered for this study. The tube had two small dents placed on opposite faces on the near-to impact end of the tube. These dents serve the purpose of a geometric imperfection, which ensures stable and progressive collapse of the tube. A linear elastic-plastic material model (MAT_PIECEWISE_LINEAR_PLASTICITY) is used to model the mild steel material. Table 3 lists the material properties. The tube is crushed axially with a rigid wall (RIGID_PLANAR_MOVING_FORCE). The rigid wall had mass of 147kg and initial velocity of 5m/s. The contact between adjacent lobes is modeled using single surface contact algorithm (AUTOMATIC_SINGLE_SURFACE) is used with coefficient of friction value 0.1. Coulomb friction coefficient on the wall is 0.3, which allows sliding along the plane of the wall.

The keyword DATABASE_BINARY_D3PLOT is used to define DT, which the time after which the results need to be saved. Larger value of DT can lead to missing of intermediate data and smaller DT will lead to higher computation time. For axial crushing of thin walled tubes, 30 microseconds are found to have small variation (less than 2%) in capturing data of interest between time steps [67]. Keyword CONTROL_TERMINATION is used to indicate analysis time. A termination time of 40ms is used for this model. Table 3.2 tabulates the results obtained from the simulations for different mesh sizes.

Table 3.2.: Simulation Results for Different Mesh Sizes

Property	3mm	2mm	1.5mm
Number of elements	9402	14402	25343
Simulation time (mins)	9	46.2	140.1
$P_{max}(KN)$	63.326	68.2	69.1
$P_m(KN)$	14.1	16.50	16.8

The fold patterns with different mesh sizes and the force vs time plots are shown in the Figures 3.5 and 3.6, respectively.

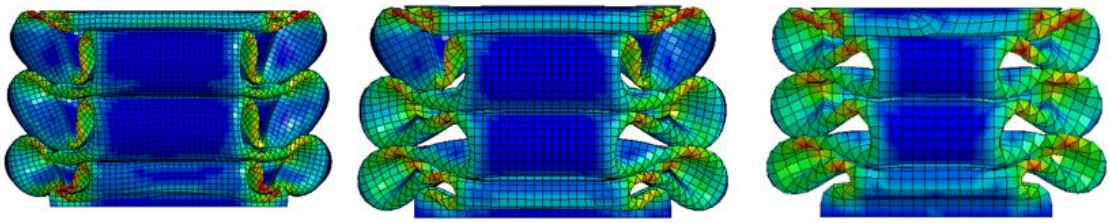

Figure 3.5.: Folding patterns for mesh sizes 1.5mm, 2mm and 3mm

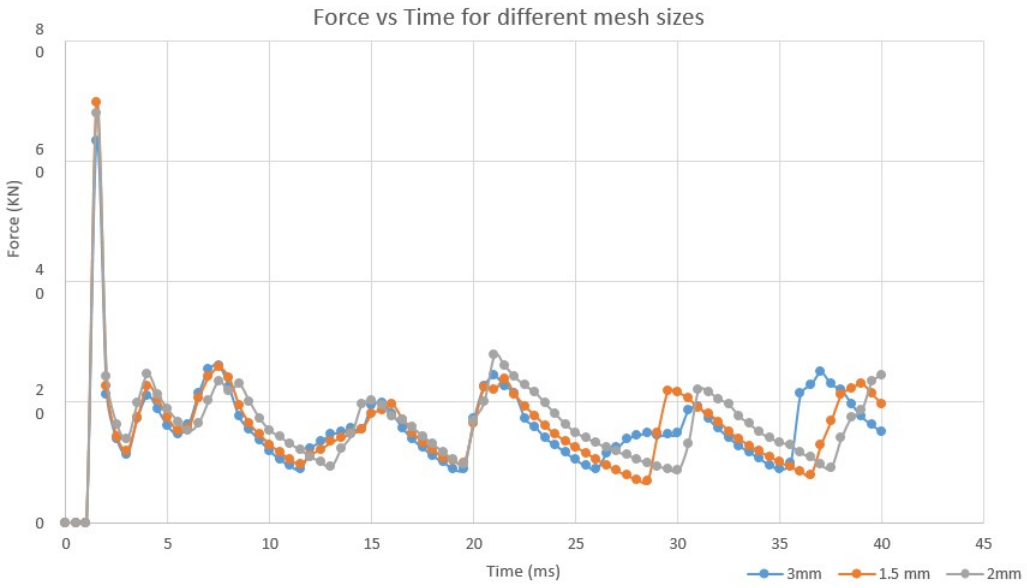

Figure 3.6.: Force vs time plot

It was observed that the folding for all the three tubes initiates from the dent and the tubes progressively collapses in symmetric mode of failure, as expected. Three lobes were formed in case of all three tubes. Also, the stress and strain distribution was similar, both qualitatively and quantitatively. Hence, it can be concluded that all the meshes show similar results in terms of location of fold formation. To obtain the convergence, further quantitative analysis is done.

According to the results tabulated in table 3.1, that the model with mesh size of 3mm underestimates the values of P_{max} and P_m. For mesh sizes 1.5mm and 2mm, the values of P_{max} and P_m are very close. It is clear that difference in values corresponding to mesh size 1.5mm and 2mm is much smaller than the difference between models with mesh size 2mm and 3mm. It is also observed that there is a drastic increase in simulation time from 2mm to 3mm. This is due to the fact that for higher resolution, time step decreases as it is dependent on the smallest element in the model in an explicit solver. The time step in parabolic system decreases by a factor of four each time the size of the smallest element is reduced by 50% [61]. Hence, due to reasonable similarities in mesh size 1.5mm and 2mm and significantly less computation time, mesh size 2mm was used for subsequent meshing of the tubes.

3.6 Validation Study

Experimental testing was done on square tubes subjected to axial dynamic loading by Abramowicz and Jones [22]. They developed theoretical models empirically to predict the axial progressive crushing of square tubes subjected to axial dynamic loading. This theoretical model gave reasonable agreement with the experimental results.

For validation of our numerical model quantitatively, this experimentally validated theoretical model is used. It should be noted that the buckling of the thin walled square tube in symmetric mode gives the qualitative validation.

Using the super folding element theory, the mean crushing force for symmetric mode

of buckling for quasi-static crushing can be calculated as:

$$P_m = 13.06\sigma_0 t^{\frac{5}{3}} b^{\frac{1}{3}} \tag{3.16}$$

The effective plastic flow rate σ_{o} can be calculated as

$$\sigma_0 = \sqrt{\frac{\sigma_y \sigma_u}{1+n}} \tag{3.17}$$

Where,

$$\sigma_{\mathrm{y}} = Yield\ stress = 253MPa$$
$$\sigma_{\mathrm{u}} = ultimate\ stress = 361MPa$$
$$n = power\ law\ exponent = 0.34$$

Substituting above values in eq.3.17, we get

σ_{o}=261.07MPa.

For our convergence study, the value of b and t were as follows:

b = 60 mm

t = 1mm

Substituting values of b and t in eq.3.16, we get,

$\mathrm{P_m}$=13.348 KN.

The material considered in our study is mild steel, the mechanical properties of which are defined in section 3.4.1. It should be noted that the stress-strain curve defines in section 3.4.1 is true stress- true strain curve for LS-DYNA's plasticity model, starting with the value at initial yield. Hence, the maximum value 608 MPa might seem to be σ_u. This is illustrated in Figure 3.7.

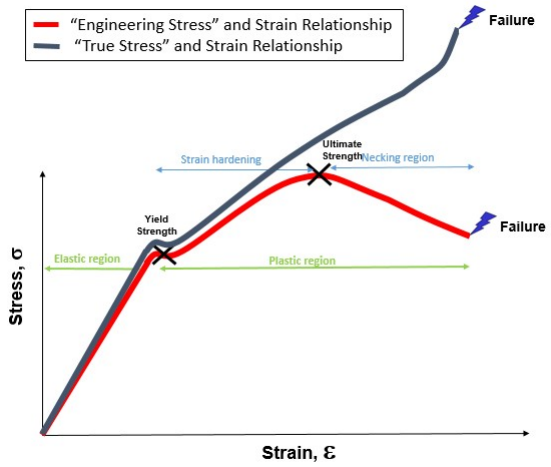

Figure 3.7.: Stress VS strain

The dynamic mean crushing force, $P_m{}^d$, and mean static crushing force, P_m, are related as [26]:

$$\frac{P_m^d}{P_m} = 1 + \left(\frac{\dot{\epsilon}}{6844}\right)^{\frac{1}{3.91}} \tag{3.18}$$

Where, $\dot{\varepsilon}$ = strain rate

For square tube with width b, buckling in symmetric mode when subjected to an impact with impactor's initial velocity V, $\dot{\varepsilon}$ is given as:

$$\dot{\epsilon} = 0.33\frac{V}{b} \tag{3.19}$$

For V=5m/s and b=60mm,

$\dot{\varepsilon}$=27.5 s^{-1}

Substituting values of P_m and $\dot{\varepsilon}$ in eq. 3.18,

$P_m{}^d$ = 16.6 KN.

Recalling that for 1.5mm, 2mm and 3mm mesh size, the numerical model predicted the value for mean crushing force as 16.8KN, 16.5KN and 14.1 KN. It is evident that the models with mesh sizes 1.5 mm and 2 mm predict the results quite accurately. Hence, it can be concluded that the Finite Element Model can accurately capture the behavior of the thin walled tubular structures under low velocity impact loading with good accuracy.

4. THIN WALLED ORIGAMI TUBE WITH DIAMOND PATTERN UNDER DYNAMIC LOADING

4.1 Pre-folding of Thin-Walled Structures

From the literature study, it is evident that the failure mode of a thin walled structure is depends on the structural profile. Out of all the failure mechanisms in thin-walled tubular structures, diamond mode is the most efficient mode of failure, which is observed when a circular tube wit D/t>100 is crushed under axial load, the reason of which will be explained later in this chapter. However, high initial buckling force is required to trigger diamond mode in circular tubes. On the other hand, comparatively low initial buckling force is required to trigger symmetric mode of failure in the square tube of similar dimensions. To overcome this problem, a square thin walled tubular structure can be pre-folded in such a manner that it buckles in diamond mode. Hence, in the event of crash, this structure will follow the pre-folded pattern and absorb the impact energy efficiently. This can be illustrated by a simple analysis of a strut under axial compression [58].

Consider a slim, straight and axially incompressible strut of length L and bending stiffness EI. It is subjected to a force P axially. It is assumed that the axial force will retain its direction and magnitude as the strut is deforming. The strut deflect into half sine curve when the axial force P hits the Euler buckling load P_E:

$$P_E = \frac{\pi^2 EI}{L^2} \tag{4.1}$$

But, if the strut is pre-folded into a curve as

$$y_0 = \delta_1 sin\frac{\pi x}{L} + \delta_2 sin\frac{2\pi x}{L} \tag{4.2}$$

Where δ_1 and δ_2 are the amplitudes of the half and full sine components, respectively. Here $\delta_1 << \delta_2$, so that the full sine component dominates.

The curvature of the strut as per the linear and small deformation analysis [68], is given by

$$\chi = \frac{d^2y}{dx^2} - \frac{d^2y_0}{dx^2} \tag{4.3}$$

The struts end shortening is given by

$$\zeta = \int_0^L \frac{1}{2}\Big[\Big(\frac{dy}{dx}\Big)^2 - \Big(\frac{dy_0}{dx}\Big)^2\Big]dx \tag{4.4}$$

The potential energy of the system is

$$V = \frac{1}{2}EI\int_0^L \Big(\frac{d^2y}{dx^2} - \frac{d^2y_0}{dx^2}\Big)^2 dx - P\int_0^L \frac{1}{2}\Big[\Big(\frac{dy}{dx}\Big)^2 - \Big(\frac{dy_0}{dx}\Big)^2\Big]dx \tag{4.5}$$

Performing the calculus of variation on V in equation 4.5

$$\delta V = \Big(-P\frac{dy}{dx}\delta y\Big) + \Big[EI\Big(\frac{d^2y}{dx^2} - \frac{d^2y_0}{dx^2}\Big)\delta\Big(\frac{dy}{dx}\Big)\Big] + \int_0^L \Big[EI\Big(\frac{d^4y}{dx^4} - \frac{d^4y_0}{dx^4}\Big) + P\frac{d^2y}{dx^2}\Big]\delta y dx \tag{4.6}$$

Applying boundary conditions for the strut at x=0 and x=L, we get

$$(y)_{(x=0)} = (y)_{(x=L)} = \Big(\frac{d^2y}{dx^2}\Big)_{(x=0)} = \Big(\frac{d^2y}{dx^2}\Big)_{(x=L)} = 0 \tag{4.7}$$

Substitute Eq. (4.7) in Eq. (4.6)

$$\delta V = \int_0^L \Big[EI\Big(\frac{d^4y}{dx^4} - \frac{d^4y_0}{dx^4}\Big) + P\frac{d^2y}{dx^2}\Big]\delta y dx \tag{4.8}$$

The equilibrium is attained when

$$EI\Big(\frac{d^4y}{dx^4} - \frac{d^4y_0}{dx^4}\Big) + P\frac{d^2y}{dx^2} = 0 \tag{4.9}$$

Performing calculus of variation on δV in Eq. (4.8)

$$\delta^2 V = \int_0^L \Big[EI\delta\Big(\frac{d^4y}{dx^4}\Big) + P\delta\Big(\frac{d^2y}{dx^2}\Big)\Big] \tag{4.10}$$

Now, to derive the deflection curve of the strut, substitute Eq. (4.2) in Eq. (4.9) and by solving Eq. (4.9)

$$y = A_1 sin\sqrt{\frac{P}{EI}}x + A_2 cos\sqrt{\frac{P}{EI}}x + A_3 x + A_4 + \frac{P_E}{P_E - P}\delta_1 sin\frac{\pi x}{L} + \frac{4P_E}{4P_E - P}\delta_2 sin\frac{2\pi x}{L} \tag{4.11}$$

Where A_1, A_2, A_3, A_4 are the constants of integration to be found.

Applying boundary conditions in Eq. (4.7), we get

$A_2 = A_3 = A_4 = 0$

and

$$A_1 sin\sqrt{\frac{P}{EI}}L = 0 \tag{4.12}$$

Solving 4.12 gives

$$A_1 = 0 \tag{4.13}$$

Which gives

$$y = \frac{P_E}{P_E - P}\delta_1 sin\frac{\pi x}{L} + \frac{4P_E}{4P_E - P}\delta_2 sin\frac{2\pi x}{L} \tag{4.14}$$

It is evident $|P_E - P|$ is comparatively large, the second term on RHS of Eq. (4.14) dominates because $\delta_1 << \delta_2$. Hence, the strut is a full sine curve after deflecting. On the other hand, when P is getting closer to P_E, the first term on the RHS dominates, resulting the deflection curve of strut to a half sine curve.

Substitute Eq. (4.14) in Eq. (4.10)

$$\delta^2 V = \frac{\pi^4 P_E^2}{2L^3}\Big(\frac{\delta_1^2}{P_E - P} + \frac{256\delta_1^2}{4P_E - P}\Big)(\delta x)^2 \tag{4.15}$$

When $P<P_E$, $\delta^2 V>0$. Hence, Eq. (4.14) represents a stable equilibrium path.
For Eq. 4.12 the other solution is

$$\sqrt{\frac{P}{EI}}L = k\pi \tag{4.16}$$

k is a positive integer. For the smallest value of k=1,

$$P = P_E \tag{4.17}$$

Substitute Eq. (4.17) in Eq. (4.11). The fourth term on RHS of Eq. (4.11) dominates, which means the strut is essentially a half sine curve on buckling.
Consider P increasing from zero. To keep the initial full sine shaped during the collapse, one way is to force the strut to yield when P is well below P_E. Hence, the first term on RHS of Eq. (4.14) becomes negligible since $\delta_1 << \delta_2$. Eq. (4.14) can be written as

$$\delta_m = \frac{4P_E}{4P_E - P}\delta_2 \tag{4.18}$$

Where, δ_m is the max deflection of the strut, which occurs at x = L/4. Also, for material yielding to take place in the strut, the deflection required is:

$$\delta_y = \frac{(\sigma_y A - P)I}{PAz} \tag{4.19}$$

Where,

A = cross section area

Z = max distance from the neutral axis on the section.

Now, quantification of this problem is necessary to make the picture clearer. Assume that the cross section of the strut is square, with dimensions L = 100 mm, I = 1/12 mm^4, A = 1mm^2, z = 0.5 mm. Also, E = 210 GPa and δ_y = 200MPa. Figure 4.1 shows the plot of δ_m and δ_y vs P. δ_2 is varied from 0.5 mm to 1.5 mm. It is evident from figure 4.1 that when δ_2 >1.32, δ_m intersects δ_y on the left side of P_E. In other words, plastic hinge develops for load applied less than critical load, indicating that the full sine cure is preserved on yielding of strut.

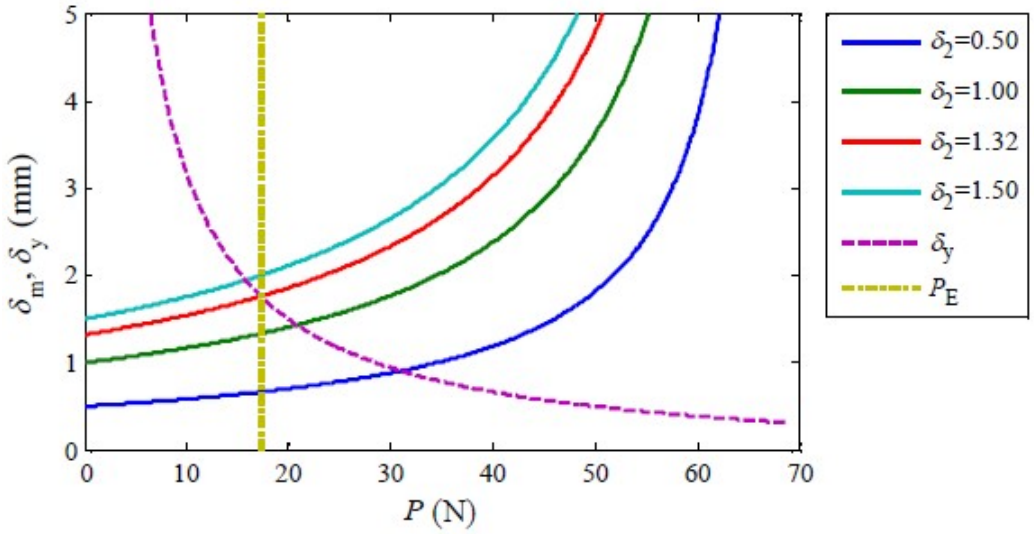

Figure 4.1.: Deflection vs load curve for pre-folded strut

If the full sine curve is preserved until the strut yields, plastic hinges will be formed at x = L/4 or 3L/4, assuming that the material to be elastic-perfectly plastic. Since the plastic hinge's stiffness is lower than that of the strut, leading to concentration of bending deformation in the plastic hinge. Now the strut looks like a two shorter struts connected by a plastic hinge. As the strut deforms axially, new plastic hinges occur. This is due to the different lengths of the two parts. This analysis shows that a pre-folded strut would have higher energy absorption than a straight one due to the formation of more plastic hinges.

Now, the next objective is to find the geometric parameters for which the pattern is developable when subjected to a low velocity impact.

4.2 Design and Geometric Analysis of Diamond Pattern

As already evident from the above analysis that pre-folding a tubular structure in such a way that it induces a specific failure mode, high EA can be achieved, provided proper pattern and geometric dimensions are chosen. It is already known that square tubular structure collapses in symmetric mode, extensional mode or mixture of both modes and circular tubes collapses in concertina mode, diamond mode or mixed mode. Both extensional mode in square tube and concertina mode in circular tube, are very efficient in terms of EA capacity, but a very high initial buckling force is required to activate these modes, which contradicts one of the requirement of a crashworthy structure. Also, these kind of collapse modes cannot be activated in thin-walled structures they bend easily rather than stretching. So, to have the advantage of low initial buckling force of a square tube and high energy absorption capacity of a circular tube, a square tube is folded using origami technique in such a way that it triggers diamond mode of failure. The pre-folded tube obtained is no more a square tube, but a complex cylindrical enclosure.

Before going to the diamond (Yoshimura) pattern, it is necessary to understand the diamond mode of failure in circular tube and why is it superior to symmetric mode of failure in terms of EA capacity. A thin walled square tube with the following dimensions: D=100mm, t=1mm, H=200mm was subjected to axial compression. It should be noted that, since D/t=100 and H/D=2, the tube is supposed to fail in diamond mode. It was observed that the tube collapses in diamond mode with 4 diamond lobes circumferentially. It collapses in such a way that the structure in the intermediate stage when the diamond lobes are visible, satisfies all the rules stated in chapter 1. Hence, origami technique best suits to pre-fold a square tube to trigger

diamond mode of collapse. Figure 4.2 shows basic pattern for the diamond mode. The solid and dashed lines represent the hills and valleys, respectively.

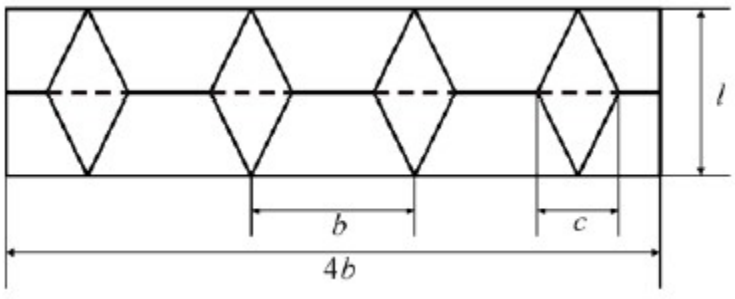

Figure 4.2.: Basic module for a diamond mode

When folded according to the defined creases, the two ends meet, giving rise to a complex cylindrical enclosure replicating the diamond mode of failure, which is illustrated in Figure 4.3. The diamond lobes induces the diamond mode of collapse and also acts as the geometric imperfection to reduce initial peak crushing force.

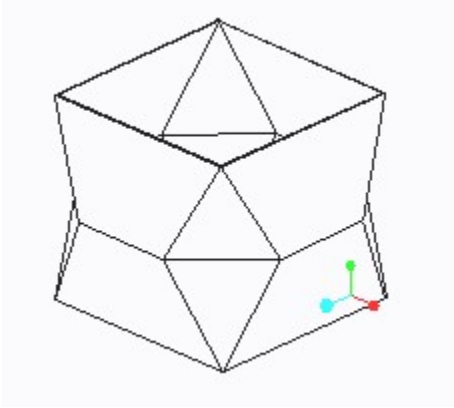

Figure 4.3.: Diamond module

The origami structure can be completely defined by three geometrical parameters, b is the width of tube, c is the width of the lobe and l is the length of the unfolded module.

The Dihedral angle 2θ can be calculated as:

$$cos\theta = (\sqrt{2} - 1)\frac{c}{l} \tag{4.20}$$

Also, following constraints on c needs to be satisfied:

c≤b, in order for the pattern to be developable.

c≤ $(\sqrt{2} + 1)l$, because cos$\theta \leq 1$.

The basic pre-folded module can be stacked in longitudinal direction to obtain a tubular structure. Also with some modifications, this pattern can be modified to design a polygonal tube, with an additional geometric parameter, N. Figure 4.4 and 4.5 illustrates the basic module for hexagonal and octagonal tube, respectively. The dihedral angle can be calculated as:

$$cos\theta = tan(\frac{\pi}{2N})\frac{c}{l} \tag{4.21}$$

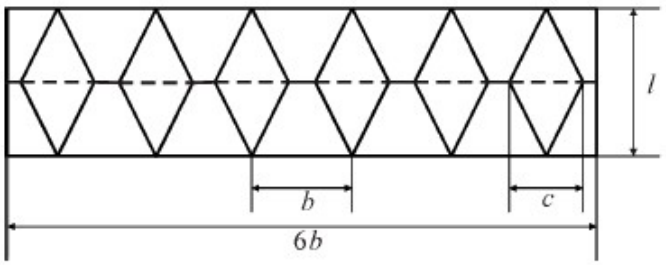

Figure 4.4.: Basic module for hexagonal diamond module

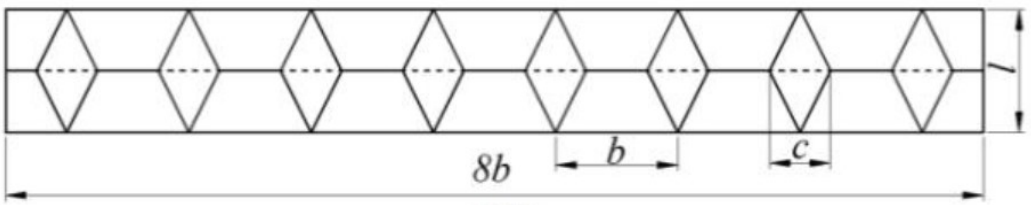

Figure 4.5.: Basic module for octagonal diamond module

4.3 Symmetric Mode vs Diamond Mode

Figure 4.6 illustrates the symmetric mode of failure and the diamond mode of failure.

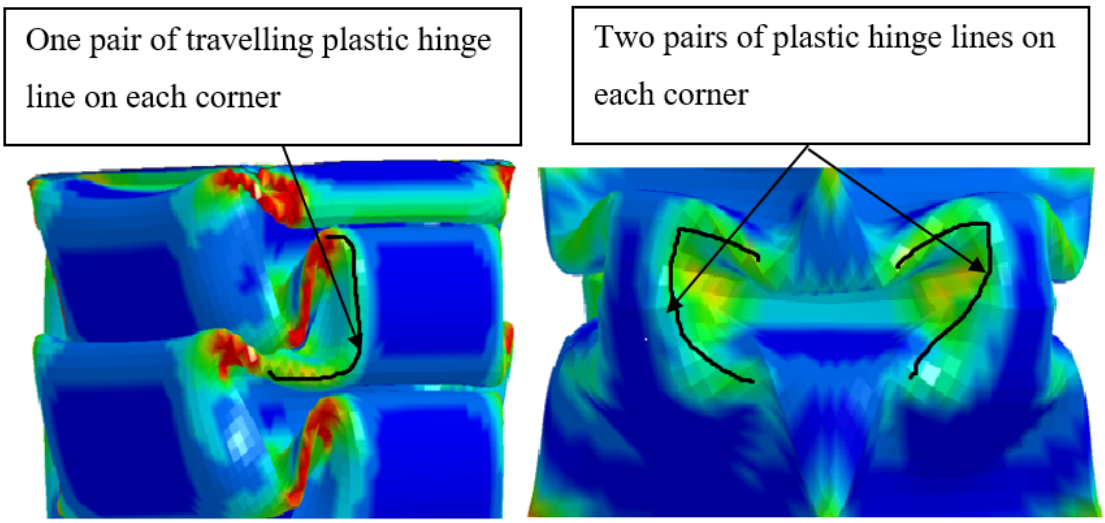

Figure 4.6.: Symmetric and diamond modes of failure

It can be observed that four pairs of travelling hinge lines are developed on each lobe in the case of square tube, and eight travelling hinge lines are developed in case of circular tube. This is the main for increase in EA, recalling that travelling hinge lines account to two- third of the total energy absorbed due to plastic deformation.

4.4 Tube Profile

As already known, polygonal tubes are tradeoff between square and circular tubes. The EA capacity of polygonal tubes increases with number of sides, until it becomes a circle. At the same the activation force increases and stability and repeatability decreases. To study the effect of profile of origami tube with diamond pattern, three

tubes with identical dihedral angle, number of modules and surface with square, hexagonal and octagonal profile are studied. The tubes are crushed axially under low velocity dynamic loading, as discussed in chapter 3. The crushing process of the three tubes is shown in Figures 4.7, 4.8 and 4.9.

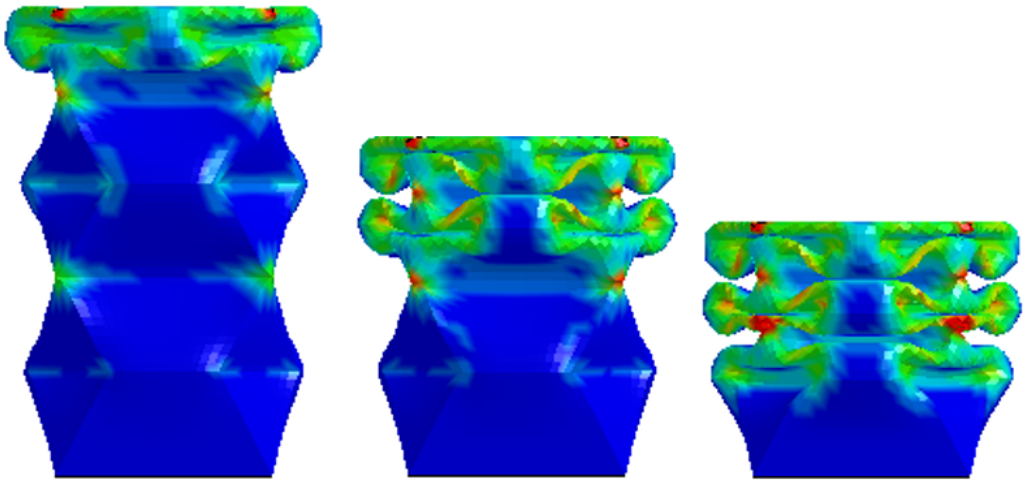

Figure 4.7.: Crushing of square tube with diamond pattern

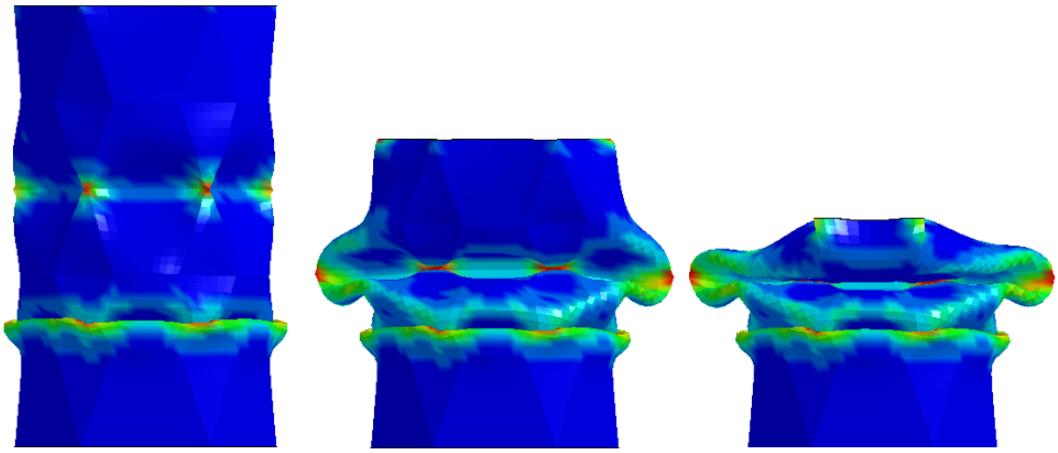

Figure 4.8.: Crushing of hexagonal tube with diamond pattern

Figure 4.10 shows the Force vs displacement plots for the three tubes.

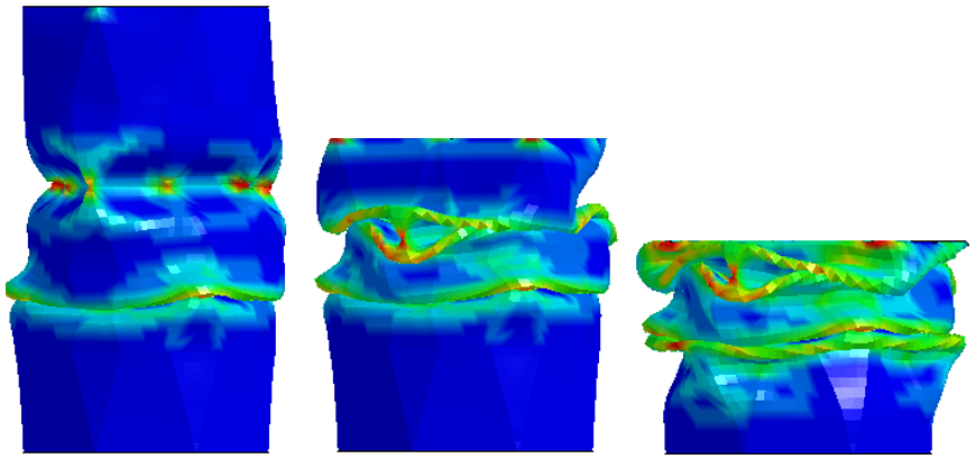

Figure 4.9.: Crushing of octagonal tube with diamond pattern

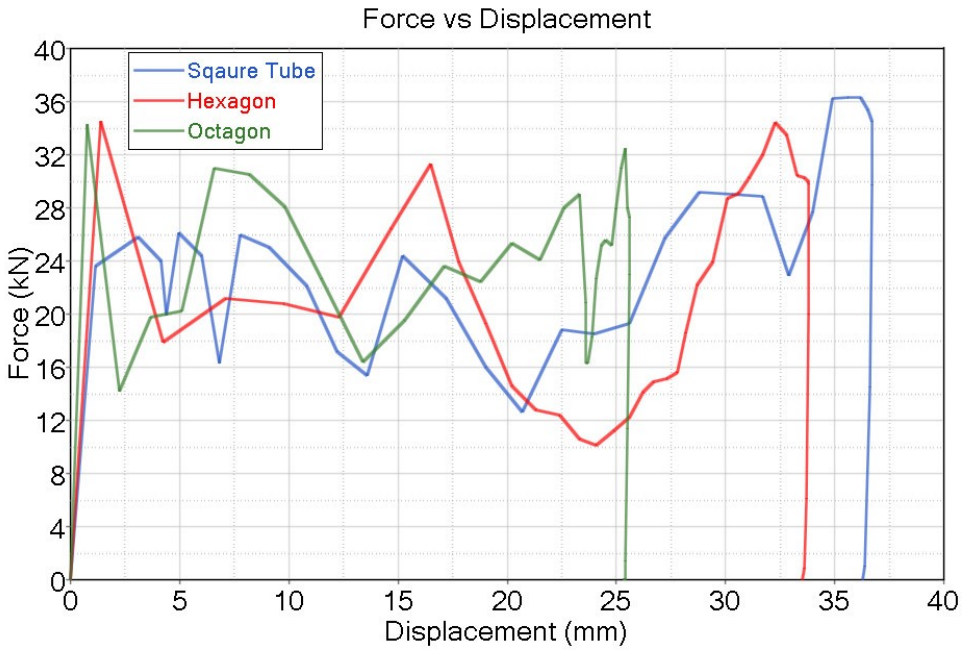

Figure 4.10.: Force vs Displacement for square, hexagonal and octagonal origami tubes.

It was observed the square origami tube follows the pre-designed pattern very well. Travelling hinge lines were induced as expected and the impact energy was absorbed in a stable manner. On the other hand, the hexagonal and octagonal tubes do not follow the pre-designed pattern.

It is evident that the initial peak crushing force is lower in case of square tube as compared to the hexagonal and octagonal tube. Also, the fringe patterns of the tube suggest that effective plastic strain is well distributed in the case of square tube as compared to the hexagonal and octagonal tube. Recalling that mostly four lobes and sometimes three diamond lobes are generate when a circular tube collapses in diamond mode [25].

This indicates that origami tube with four diamond lobes will perform well as an energy absorption device.

4.5 Parametric Study

In this work, square tubes pre-folded diamond pattern on it, are studied extensively to investigate the effect of geometric parameters on the performance of the tube crushed axially under dynamic loading. Forty Eight origami tube configurations were studied. All the origami tubes had same b and surface area same as the conventional tube. The origami tubes were made by varying c, l and t. All the parameters are varied in increments. The nomenclature is as follows, 'O- dihedral angle - no. of modules - b/t ratio'. For example, a tube with dihedral angle 2θ=172 degrees, 5 modules and b/t= 60 will be named as 'O-172-5-60'.

The tubes are arranged based on b/t, number of modules (l/b) and the dihedral angle 2θ. It should be noted that the number of modules depend on the l/b ratio, where l is the length of the unfolded module and b is the length of the side of the tube, as shown in Figure 4.1. They share an inverse proportionality. Figures 4.11, 4.12 and 4.13 lists the tube configurations and results for initial peak crushing force, mean crushing force, crush force efficiency and maximum intrusion of wall. Here, D, IDM, FM and NTEPF indicates complete diamond mode, incomplete diamond mode, failure mode and near to impact end progressive folding, respectively.

Model name	c (mm)	l (mm)	l/b	2θ	Pi (KN)	Pm (KN)	Pi/Pm	FM	NTEPF	Max intrusion (mm)
O-156-3-50	33.335	66.67	1.3334	156	29.5	17.3	1.705202	PNF	NO	49.9
O-160-3-50	26.668	66.67	1.3334	160	31.56	20.7	1.524638	IDM	NO	90.87
O-164-3-50	22.22111	66.67	1.3334	164	32.5	21.2	1.533019	IDM	NO	88.419
O-168-3-50	16.6675	66.67	1.3334	168	33.83	20.8	1.626442	IDM	NO	86.007
O-156-4-50	25	50	1	156	28.45	21.2	1.341981	D	YES	83.355
O-160-4-50	20	50	1	160	29.733	22.4	1.327366	D	YES	79.15
O-164-4-50	16.665	50	1	164	30.517	21.1	1.446303	D	YES	80
O-156-4-50	12.5	50	1	168	32.711	20.9	1.565120	PNF	YES	79.2
O-156-5-50	20	40	0.8	156	27.117	21.3	1.273099	D	YES	83.3
O-160-5-50	16	40	0.8	160	28.04	20.1	1.395025	D	YES	79.3
O-164-5-50	13.332	40	0.8	164	28.508	19.2	1.484792	IDM	YES	87
O-168-5-50	10	40	0.8	168	29.004	20.1	1.442985	PNF	YES	86.865
O-156-6-50	16.6665	33.333	0.6667	156	27.836	21.3	1.306854	D	YES	83.1
O-160-6-50	13.3332	33.333	0.6667	160	27	21.9	1.232877	D	YES	78.15
O-164-6-50	11.10989	33.333	0.6667	164	28.55	20.8	1.372596	D	YES	81.522
O-168-6-50	8.33325	33.333	0.6667	168	30.956	21.8	1.420000	D	YES	80.81

Figure 4.11.: Tube configurations and results: b/t=50

Model name	c (mm)	l (mm)	l/b	2θ	PCF (KN)	Pm (KN)	Pi/Pm	FM	NTEPF	Max intrusion (mm)
O-156-3-55	33.335	66.67	1.3334	156	25.37	16.66	1.522809	IDM	NO	106.99
O-160-3-55	26.668	66.67	1.3334	160	27.429	16.8	1.632679	D	NO	106.91
O-164-3-55	22.22111	66.67	1.3334	164	28.34	17	1.667	D	NO	104.55
O-168-3-55	16.6675	66.67	1.3334	168	29.24	17.2	1.7	D	No	99.439
O-156-4-55	25	50	1	156	24.785	17.8	1.392416	D	YES	99.676
O-160-4-55	20	50	1	160	25.74	19.3	1.333679	D	YES	95.479
O-164-4-55	16.665	50	1	164	26.433	18.7	1.413529	D	YES	94.164
O-156-4-55	12.5	50	1	168	29.386	18.6	1.579892	D	NO	94.331
O-156-5-55	20	40	0.8	156	23.386	19.4	1.205464	D	YES	97.487
O-160-5-55	16	40	0.8	160	24.52	18.6	1.31828	D	YES	100
O-164-5-55	13.332	40	0.8	164	25.014	17.6	1.42125	D	YES	102.58
O-168-5-55	10	40	0.8	168	25.57	18.3	1.397268	PNF	NO	99.845
O-156-6-55	16.6665	33.333	0.6667	156	23.147	19	1.218263	D	YES	96.881
O-160-6-55	13.3332	33.333	0.6667	160	23.53	20.1	1.170647	D	YES	93.165
O-164-6-55	11.10989	33.333	0.6667	164	24.79	19.5	1.271282	D	YES	94.43
O-168-6-55	8.33325	33.333	0.6667	168	26.99	20	1.3495	D	YES	92.8

Figure 4.12.: Tube configurations and results: b/t=55

The study includes two things, first, whether the pattern is followed, and second, the peak and mean crushing force. The axial crushing was simulated using the developed FEA model. All tubes were modeled and simulated with the same approach as explained in chapter 3.

Model name	c (mm)	l (mm)	l/b	2θ	PCF (KN)	Pm (KN)	Pi/Pm	FM	NTEPF	Max intrusion (mm)
O-156-3-60	33.335	66.67	1.3334	156	22.5	14.8	1.52027	IDM	NO	119.4
O-160-3-60	26.668	66.67	1.3334	160	24.517	15.6	1.571603	IDM	NO	119.49
O-164-3-60	22.22111	66.67	1.3334	164	25	14.9	1.6778	PNF	NO	118.73
O-168-3-60	16.6675	66.67	1.3334	168	25.9	15.2	1.703947	IDM	NO	116.93
O-156-4-60	25	50	1	156	22.33	17.1	1.305848	D	YES	111.19
O-160-4-60	20	50	1	160	22.6	17.4	1.298851	D	YES	109.35
O-164-4-60	16.665	50	1	164	23.19	17.83	1.4	D	NO	109.94
O-156-4-60	12.5	50	1	168	25.288	17.9	1.412737	D	NO	108.11
O-156-5-60	20	40	0.8	156	20.77	16.6	1.251205	D	YES	110.96
O-160-5-60	16	40	0.8	160	21.65	16.3	1.328221	D	YES	112.3
O-164-5-60	13.332	40	0.8	164	22.005	15.6	1.410577	PNF	NO	119.23
O-168-5-60	10	40	0.8	168	22.62	16.2	1.396296	PNF	NO	111.55
O-156-6-60	16.6665	33.333	0.6667	156	20.18	17.2	1.173256	D	YES	110.18
O-160-6-60	13.3332	33.333	0.6667	160	20.79	17.7	1.174576	D	YES	106.18
O-164-6-60	11.10989	33.333	0.6667	164	22.25	18.2	1.222	D	YES	106.89
O-168-6-60	8.33325	33.333	0.6667	168	23.28	18	1.25	D	YES	105.02

Figure 4.13.: Tube configurations and results: b/t=60

4.6 Results and Discussion

4.6.1 Effect of Dihedral Angle 2θ and Number of Modules (l/b)

Dihedral angle is the angle between the two faces in the un-deformed diamond lobe. Figure 4.2 illustrates the dihedral angle. The dihedral angle 2θ depends on the ratio c/l (Eq. 2.20). It is decreases with increase in c/l ratio. It is a very important parameter which influences the fact whether the pre-folded pattern is followed or not and the propagation of plastic hinge lines. A straight square tube can be considered as an origami tube with dihedral angle equal to 180 degrees. Hence, higher value of dihedral angle will lead to high peak crushing forces associated with them. Also, the probability that the pattern will follow decreases. On the other hand, if the dihedral angle is too small, the pattern will be followed, but the down side is that the area swept by the travelling plastic hinges will be less and there will also be a considerable reduction in the rotation of stationary plastic hinges, which is undesirable from the energy absorption point of view.

The number of modules M depend on the l/b ratio. As l/b increases, the number of modules decrease. In this study, the total un-folded total length of the tube and length of each side, b, is kept same for all the tubes. The l/b value is varied by varying l. The value of l is selected such that the value of M is a natural number. The ratio l/b is an important factor which influences energy absorption characteristics of the tube. It can be predicted that smaller value of l/b i.e. higher number of modules will lead to more energy absorption due to higher number of stationary plastic hinges. But, very small value of l/b will make the structure complex and also the lead to overriding of the pattern. Due to this, many plastic hinge lines will go unactivated, leading to decrease in energy absorption.

Forty Eight origami tubes are studied here. They are subjected to low velocity impact. The rigid wall subjected to an initial velocity of 5 m/s and is allowed to come to rest. The effect of number of modules and dihedral angle is studied for three different thickness values i.e. b/t ratio.

For 3 Modules (l/b = 1.3334):

The buckling mode is studied starting with M=3 (l/b = 1.334). The dihedral angle 2θ was varied from 156 degrees to 168 degrees with an increment of four degrees for three different wall thicknesses, leading to a total of twelve configurations. The results from the simulation show that the pattern is not followed in majority of the cases. In none of the tubes, the folding starts from near to impact end. The buckling begins at the central module and propagates in either direction. The pattern was not followed for O155-3-50, and O164-3-60. All tubes having b/t = 55, i.e. O156-3-55, O160-3-55, O164-3-55 and O168-3-55, failed in a complete diamond mode. Rest of the tubes failed in incomplete diamond mode, where the pattern is followed, but the modules are underdeveloped.

For 4 Modules (l/b = 1):

Similar study is performed for tubes with 4 modules. For b/t = 50, it was seen that the predefined pattern is followed well for 2θ from 156 degrees to 164 degrees.As 2θ reaches, the buckling is initiated from the third module and progresses towards the second. But due to underdeveloped collapse pattern, the tube buckles globally as the buckling process proceeds.

For b/t = 55, all tubes buckle in complete diamond mode. For tubes O156-4-55, O160-4-55 and O164-4-55, the buckling initiates from the first module, which is the near to impact end. For O168-4-55, the buckling is initiated from the third module and propagates towards the second. This is illustrated in figure 4.1a-c.

For b/t = 60, similar trend is observed as that for b/t = 55. All the tubes follow the predefined pattern and fail efficiently in diamond mode, without any underdeveloped pattern. For tubes O156-4-60 and O160-4-60, the buckling initiates from near to impact end. For O164-4-55 and O168-4-55, the buckling propagation is similar to that of O164-4-55.

For 5 Modules (l/b = 0.8):

For b/t = 50, tubes O156-5-50 and O160-5-50 buckle in full diamond mode with buckling initiating from near to impact end. O164-5-50, it is observed that first module follows the pattern and buckles in complete diamond mode. However the pattern is not followed for the second module. The travelling plastic hinge lines are not developed completely, hence there is excess and uneven rotation of stationary plastic hinge lines, leading to underdeveloped pattern. For O168-5-50, the pattern is not at all followed and it buckles in a much undesired pattern.

For b/t = 55, the tubes with 2θ from 156 degrees to 164 degrees buckle in complete diamond mode. The buckling also initiates from near to impact end. As 2θ reaches 168 degrees, the tube no more follows the pre-folded pattern.

For b/t = 60, compete diamond mode is achieved for tubes with 2θ equal to 156 degrees and 160 degrees, with buckling initiation from near to impact end. As 2θ reaches 164 degrees the pattern is no more followed.

For 6 Modules (l/b = 0.667):

All the configuration in this category buckle in complete diamond mode with buckling initiation from near to impact end.

Following conclusion can be drawn from the obtained results:

- For 3 modules i.e. l/b = 1.334, in most cases the pattern is either not followed or is underdeveloped. This might be due to the fact that the length of the module is greater than the width of the tube, making it slender enough for the tube to not follow the predefined pattern. But in case of l/b $\leq$ 1, the pattern is followed my majority of the tubes. This indicates that l/b >1 does not produce desirable results. Also, it should be noted that four lobes are formed when the identical straight square tube was crushed and the trend of following pattern by tubes with four modules or more, might have a strong correlation. It should be noted that it is the l/b ratio and not the number of modules responsible for such behavior. Origami tubes with 3 modules and l/b = 1 would behave in another manner than the discussed above.

- For 4 modules or more, the pattern is well followed for 2θ from 156 degrees to 164 degrees. As 2θ reaches 164 degrees, in majority of cases the pattern is underdeveloped or the pattern is not followed completely. The distinguishing between complete diamond mode and incomplete diamond mode is completely based on visual inspection. If the area swept by the travelling plastic hinges is less than what it should have, it is considered incomplete diamond mode.

4.6.2 Energy Absorption Properties

All the results from the simulations are quantified in table 4.1. First observation made was, that for same number M modules and b/t, Pmax i.e. initial peak crushing force increases with increase in the dihedral angle 2θ, provided the tube follows the pre-folded pattern. This is due to the fact that higher energy is required to activate the pre-folded pattern as the dihedral angle approaches 180 degrees. This trend is illustrated in Figures 4.14, 4.15 and 4.16.

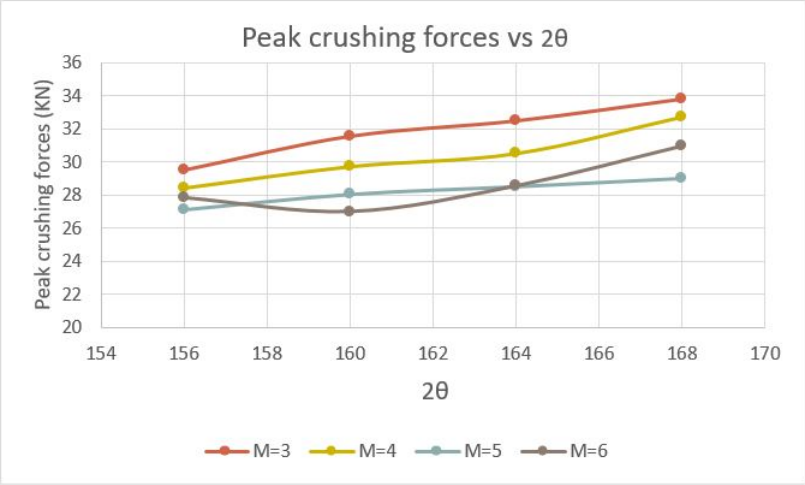

Figure 4.14.: PCF vs 2θ for b/t=50

Secondly, a different trend is observed in case of mean crushing force, P_m. For all M's except M = 5, as the dihedral angle increases, in majority of cases, the mean crushing force increases for the same number of modules M and b/t from 2θ equal from 156 degrees to 160 degrees and the drops down slightly. This drop is mainly due to underdeveloped pattern or if the pattern is not followed at all. For example, for b/t = 55 and M = 5, the mean crushing force rises from 2θ equal from 156 degrees to 160 degrees and then drops due to underdeveloped pattern and pattern not followed for 2θ equal to 164 degrees and 168 degrees, respectively.

But, for b/t = 55 and M = 6, even though the trend is followed, the rise and drop is not significant. This is because all four tubes fail in complete diamond mode. M = 5 shows a different trend for all b/t ratios.

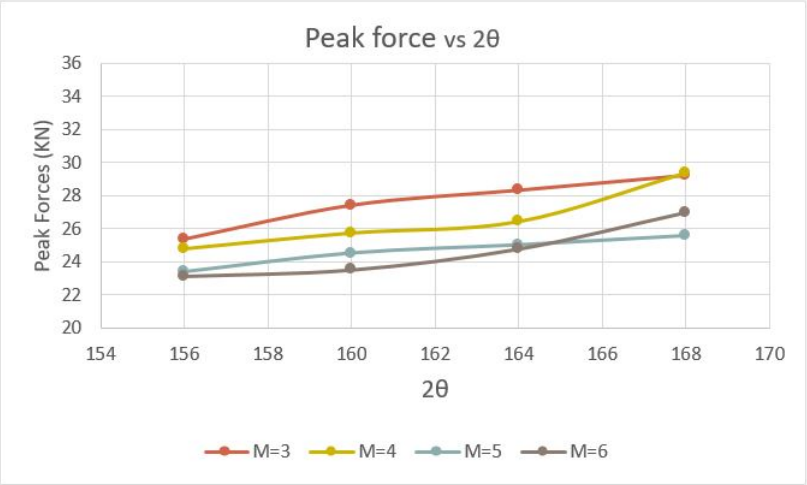

Figure 4.15.: PCF vs 2θ for b/t=55

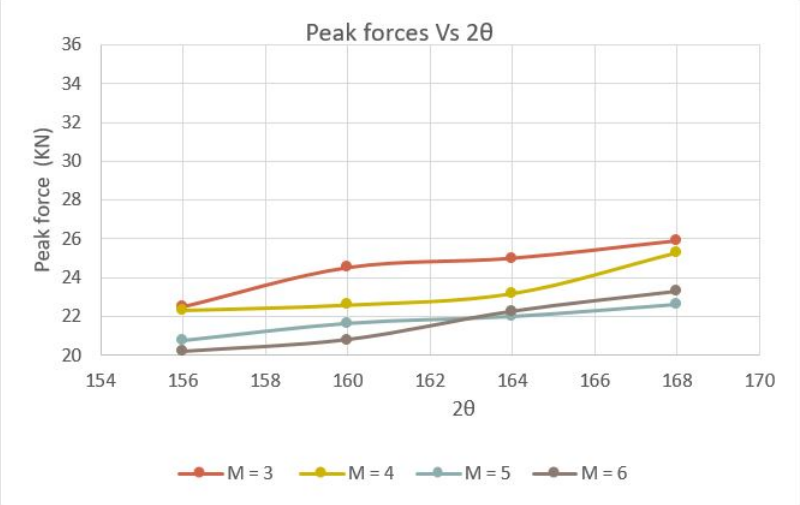

Figure 4.16.: PCF vs 2θ for b/t=60

The mean crushing force drops from 2θ equal to 156 degrees and 164 degrees and increases slightly for 2θ equal to 168 degrees.

Thirdly, for same value of dihedral angle 2θ, the initial peak crushing force drops as the number of modules M increases. But the mean crushing force varies randomly.

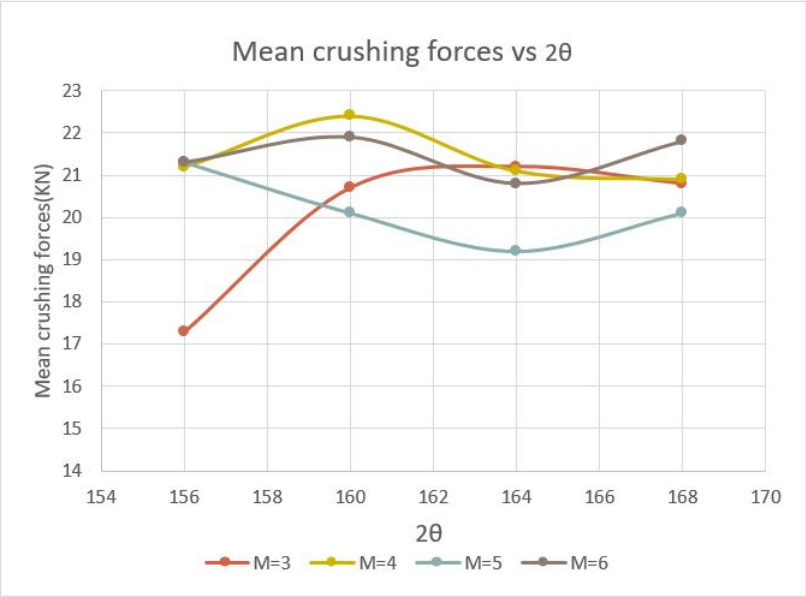

Figure 4.17.: Mean Crushing Force vs 2θ for b/t=50

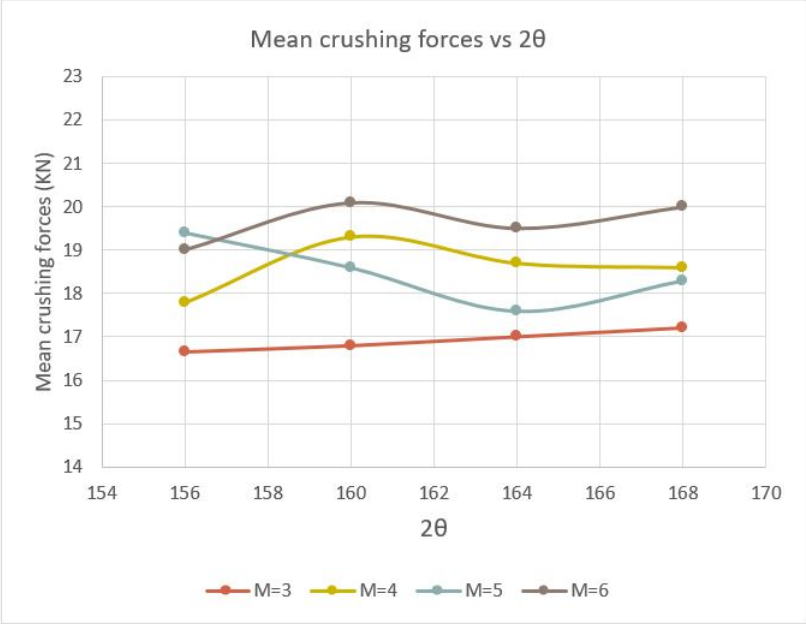

Figure 4.18.: Mean Crushing Force vs 2θ for b/t=55

Fourthly, it is observed that when the modules are underdeveloped or the pattern is not followed, there is a drop in mean crushing force, leading to decrease in energy absorption. This is because less area is effectively swept by the travelling plastic hinges and the reduction in the rotation of stationary plastic hinges.

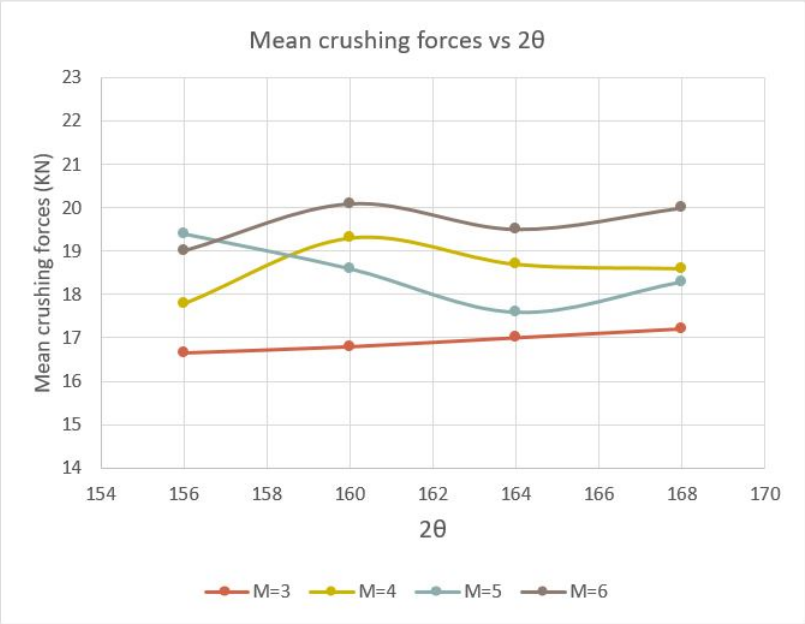

Figure 4.19.: Mean Crushing Force vs 2θ for b/t=60

Finally, it was observed that the thickness did not affect the results significantly. The trends are also similar for different b/t ratios. This indicates that the pattern is developable for the selected b/t range.

4.7 Tube With Progressive Stiffness

From the study of the origami tubes under low velocity impact, it was observed that the behavior of the structure was uniform throughout since all the modules in a single tube were identical. So if a tube with identical module is used, it will not be able to adapt to varying loading conditions. Also, the collapse does not initiate from near to impact end in many cases. This is undesirable for applications where progressive buckling from near to impact end to the back end is desired. For example the damage

for low velocity frontal impact in automobiles can be restricted to the bumper beam and crashbox. If the crashbox collapses in a progressive manner from front to back without jamming [56]. This safeguards the expensive components like front frame-rail, engine-hood and cooling system behind them. This idea is basically inspired from nature. For example, bamboos and bones have specifically graded distribution of number or cell size to adapt to their expected service environment [69, 70].

In the literature review, it was seen that one of the methods to increase energy absorption and reduce peak crushing forces was to have a graded functionally graded stiffness by varying the thickness of the tube along the length of the tube or in circumferential direction. Both tubes showed enhanced performance [55]. Generally, functionally graded structures are developed by changing mass density or the thickness. However, it is possible to achieve graded stiffness by varying the geometric parameters of the pattern along the tube. From the numerical results, it is also evident that the all combinations of l/b, b/t and 2 have different stiffness values. Hence using the results so obtained, it is possible to generate an origami tube with functionally graded stiffness. This can be achieved by using Non-dominant Sorting Genetic Algorithm to find the proper gradient as required for the application. Various surrogate models can be used to formulate the required objective functions. The advantage of this method is that tuned and enhanced performance can be achieved and these structures can be made out of a single sheet having uniform thickness, making the manufacturing less complex as compared to that of tubes with functionally graded stiffness.

To demonstrate this, a simple case is taken. The dynamic axial crushing behavior of an origami tube with three modules and l/b = 1 having varying dihedral angle 2θ is studied. From the results obtained from the parametric study, it is evident that the stiffness of the modules increases with dihedral angle 2θ. The modules are stacked in such a way that the module near to the impact end has lower 2θ and increases gradually for the other two.

The first, second and third modules are assigned the value of dihedral angle 2θ equal to 156 degrees, 160 degrees and 164 degrees, respectively. It is observed that the crushing begins from the less stiff module, which is near to the impact end. Once the maximum area was swept by the travelling plastic hinge lines for the first module, the collapse of second was initiated and similarly for the third one.

Figures 4.20 illustrates the crushing behavior of the tube. The FVD plot, Figure 4.21, illustrates the effect of progressive stiffness.

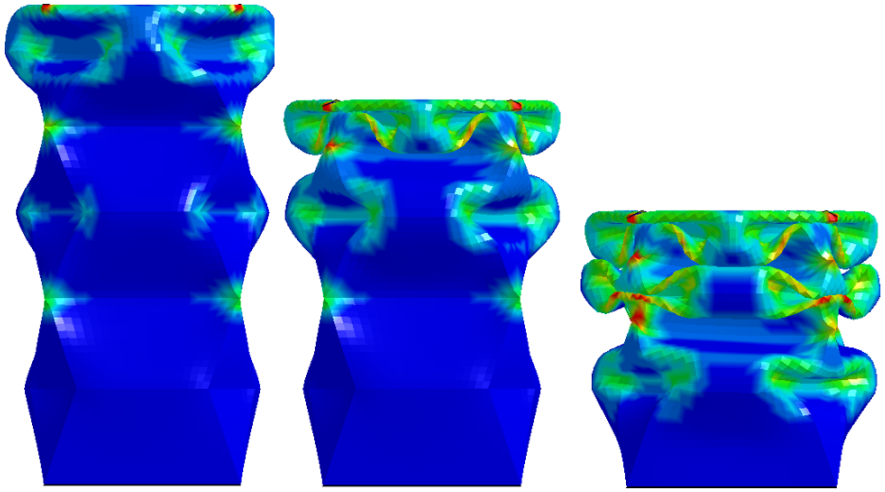

Figure 4.20.: Crushing of origami tube with graded stiffness

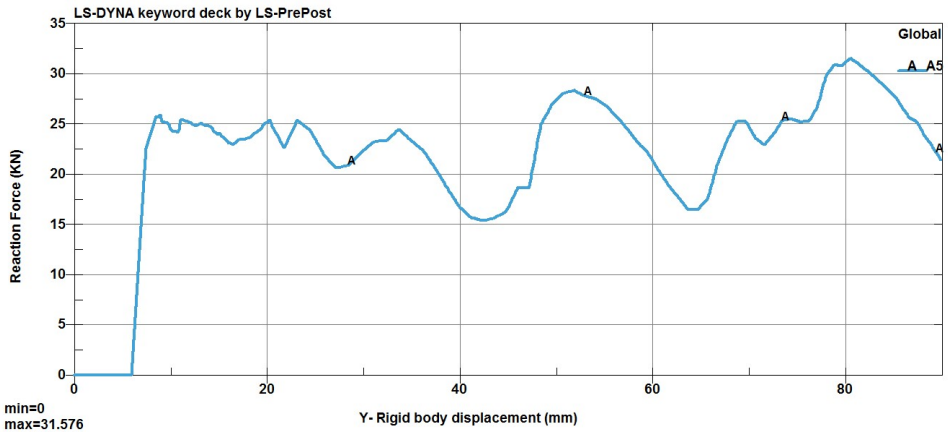

Figure 4.21.: FVD plot

Low initial peak crushing forces are achieved. As the collapse progresses, due to progressive stiffness, the force required for the collapse increases gradually and hence the maximum intrusion of the wall reduces. Also, the area under the curve increases, which leads to increase in energy absorption capacity. Hence, it can be concluded that due to the progressive stiffness, progressive collapse from near to impact end, reduction in initial peak crushing forces and increase in energy absorption capacity is achieved.

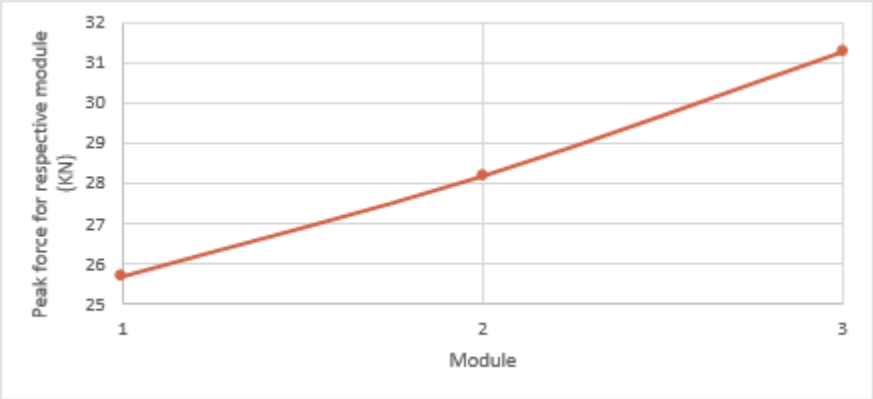

Figure 4.22.: Peak forces for respective module

From Figure 4.22, it is evident that the progressive stiffness attained in this case is linear having random gradient. However, it is possible to obtain an optimal gradient, which will further enhance the performance of the device. A parametric study of tubes with various combinations of modules with varying parameters must be conducted to achieve various gradients. Then a surrogate model for the FEA models should be developed to formulate the objective functions like Initial peak crushing force, maximum wall intrusion, SEA etc. Further, a search algorithm, like the Non-dominant Sorting Genetic Algorithm must be used to find the optimal gradient.

Hence, Origami tubes with functionally graded stiffness have immense potential as energy absorption devices.

5. SUMMARY AND FUTURE WORK

5.1 Summary

In this thesis, the axial crushing behavior of the diamond pattern was studied under low velocity impact and a methodology for developing a thin walled diamond tube with functionally graded stiffness is proposed for future work. The main accomplishments are summarized below.

An extensive literature review of basic collapse modes of square and circular tubes under various loading conditions was done. It was found that thin-walled square tubes with b/t ratio more than 40.8 buckle under symmetric mode of failure and circular tubes with D/t ratio greater than 100 buckle in the diamond mode of failure. A comparative study of axial buckling of identical square and circular tubes reveal that the diamond mode is much more efficient compared to the symmetric mode of failure. The only problem associated with diamond mode of failure is high initial peak force and the stability of the collapse.

This shortcoming was overcome by Ma [58] by pre-folding the square tube into a specific origami pattern (Yoshimura pattern) which replicate diamond mode of failure on the square tube. This reduces the initial peak crushing forces by acting as failure inducer and enhances the energy absorption capacity by doubling the travelling plastic hinges. But this is true only in the case when the predefined pattern is followed during crushing.

The first thing to do was to develop a Finite Element Model for simulating thin-walled structures under low velocity dynamic loading. By using proper governing equations and constitutive laws, appropriate element formulation, initial and boundary condition and proper discretization of space and time, an accurate numerical

model is developed for conducting this study. Since, in many application energy absorbing components like thin walled tubes are designed for impact loading, an extensive numerical study of the square tubes with predesigned diamond pattern with various configurations subjected to low velocity impact loading is carried out. The results dictate that if the collapse mode is induced, both low peak crushing force and high energy absorption is achieved. First, the origami tubes with different cross sections were studied. It was observed that the collapse mode is much repetitive and stable in case of square tube compared to hexagonal and octagonal cross sections. Then, a parametric study was conducted to study the effect of geometric parameters on the crash performance of the tubes. It was found that by selecting proper values of geometric parameters, high energy absorption can be achieved. Finally, a methodology to develop an origami tube with functionally graded stiffness is proposed for future work.

5.2 Future Work

- **Expansion of Domain of Study:**

  In this study, three parameters, i.e. the dihedral angle, number of modules and b/t ratio, were taken into consideration, with each having four values. Additional parameters like c/b ratio should be taken into consideration for the study. Also, square profile is assumed in this problem. Rectangular profile can be explored, which also increases the number of parameters.

- **Study Oblique Loading Condition with Different Loading Angles:**

  This study includes the crushing of the tubes under pure axial loading. But in real life, these structures are subjected to complex loading conditions. Hence, it is important to evaluate the performance of the origami tubes under oblique crushing.

- **Define a Multi-objective Crashworthiness Problem:**
  Since crashworthiness is a multi-objective problem, peak crushing force and maximum intrusion can be defined as objective function and an enhanced pareto can be obtained for the conflicting objectives. To do this, first it is required to fit an accurate surrogate model for the crash models. This data can be also used in machine learning and predicting Progressive Collapse Index (PCI).

- **Design a Full Bumper System with Front Rail:**
  The origami tube can be integrated with bumper beam and s-rail to evaluate the performance of the tubes in realistic complex loading scenario.

- **Develop Origami Structure with Functionally Graded Stiffness:**
  The tubes studied here have identical modules stacked on one another. Due to this, the behavior cannot adapt to varying loading condition. A structure with proper functionally graded stiffness can be designed using the obtained data, which will have the ability to adapt to loading condition.

- **Develop a Theoretical Model:**
  A theoretical model can be developed for dynamic crushing of origami tube under axial dynamic loading using kinematically admissible methods. The equations developed here can be used to modify the results from simple quasi-static crushing to predict the complex dynamic crushing behavior.

REFERENCES

REFERENCES

[1] N. H. T. S. Administration *et al.*, "2010 motor vehicle crashes: Overview," *US Department of Transportation, Washington, DC, Research Note DOT HS*, vol. 811, p. 552, 2012.

[2] P. Du Bois, C. C. Chou, B. B. Fileta, T. B. Khalil, A. I. King, H. F. Mahmood, H. J. Mertz, J. Wismans, P. Prasad, and J. E. Belwafa, "Vehicle crashworthiness and occupant protection," *Citeseer*, vol. 1, pp. 1–10, 2004.

[3] P. M. (2004) World report on road traffic injury prevention. Last accessed 15th March 2019. [Online]. Available: https://www.who.int/violence_injury_prevention/publications/road_traffic/world_report/en/

[4] I.I.H.S. (2018) General statistics for fatality facts. Last accessed 15th March 2019. [Online]. Available: https://www.iihs.org/topics/fatality-statistics/detail/yearly-snapshot

[5] A. Alghamdi, "Collapsible impact energy absorbers: an overview," *Thin-walled structures*, vol. 39, no. 2, pp. 189–213, 2001.

[6] G. Lu and T. Yu, "Energy absorption of structures and materials," vol. 1, pp. 144–172, 2003.

[7] L. Bailey, "Lambert a new claim for america's first gasoline automobile," *Antiq. Automob*, vol. 24, pp. 340–400, 1960.

[8] T. P. Hovorun, K. V. Berladir, V. Pererva, S. Rudenko, and A. Martynov, "Modern materials for automotive industry," *Journal of Engineering Sciences*, vol. 4, pp. 8–18, 2017.

[9] D. Patrascu. (2018) Crash-test cars at 62 mph in new safety facility. Last accessed 18th March 2019. [Online]. Available: https://www.autoevolution.com/news/volkswagen-to-crash-test-cars-at-62-mph-in-new-safety-facility-124364.html

[10] D. Basile. (2016) How the ancient art of origami is inspiring cutting edge technology. Last accessed 24th March 2019. [Online]. Available: https://techcrunch.com/2016/06/27/

[11] H. Koshiro. (2016) Origami construction. Last accessed 25th March 2019. [Online]. Available: https://origami.ousaan.com/library/conste.html

[12] M. C. Neyrinck and S. F. Shandarin, "Tessellating the cosmological dark-matter sheet: origami creases in the universe and ways to find them," *arXiv preprint arXiv:1207.4501*, vol. 1, pp. 3–6, 2012.

[13] T. C. Hull, "Counting mountain-valley assignments for flat folds," *arXiv preprint arXiv:1410.5022*, vol. 65, pp. 175–188, 2003.

[14] B. Cipra, E. D. Demaine, M. L. Demaine, and T. Rodgers, "Tribute to a mathemagician," *CRC Press*, vol. 1, pp. 223–241, 2004.

[15] X. Garcia. (2015) Tessellation and miura folds. Last accessed 25th March 2019. [Online]. Available: https://www.sciencefriday.com/educational-resources/tessellation-and-miura-folds/

[16] N. Turner, B. Goodwine, and M. Sen, "A review of origami applications in mechanical engineering," *Proceedings of the Institution of Mechanical Engineers, Part C: Journal of Mechanical Engineering Science*, vol. 230, no. 14, pp. 2345–2362, 2016.

[17] N. Jones and W. Abramowicz, "Static and dynamic axial crushing of circular and square tubes," in *Metal forming and impact mechanics*. Elsevier, 1985, pp. 225–247.

[18] T. Wierzbicki and W. Abramowicz, "On the crushing mechanics of thin-walled structures," *Journal of Applied mechanics*, vol. 50, no. 4a, pp. 727–734, 1983.

[19] W. Abramowicz and N. Jones, "Dynamic progressive buckling of circular and square tubes," *International Journal of Impact Engineering*, vol. 4, no. 4, pp. 243–270, 1986.

[20] D. Karagiozova, G. Nurick, and S. C. K. Yuen, "Energy absorption of aluminium alloy circular and square tubes under an axial explosive load," *Thin-walled structures*, vol. 43, no. 6, pp. 956–982, 2005.

[21] T. Reddy and S. Reid, "Axial splitting of circular metal tubes," *International Journal of Mechanical Sciences*, vol. 28, no. 2, pp. 111–131, 1986.

[22] W. Abramowicz and N. Jones, "Dynamic axial crushing of square tubes," *International Journal of Impact Engineering*, vol. 2, no. 2, pp. 179–208, 1984.

[23] K. Andrews, G. England, and E. Ghani, "Classification of the axial collapse of cylindrical tubes under quasi-static loading," *International Journal of Mechanical Sciences*, vol. 25, no. 9-10, pp. 687–696, 1983.

[24] S. Guillow, G. Lu, and R. Grzebieta, "Quasi-static axial compression of thin-walled circular aluminium tubes," *International Journal of Mechanical Sciences*, vol. 43, no. 9, pp. 2103–2123, 2001.

[25] W. Abramowicz and N. Jones, "Dynamic axial crushing of circular tubes," *International Journal of Impact Engineering*, vol. 2, no. 3, pp. 263–281, 1984.

[26] A. A. Singace and H. El-Sobky, "Behaviour of axially crushed corrugated tubes," *International Journal of Mechanical Sciences*, vol. 39, no. 3, pp. 249–268, 1997.

[27] S. Lee, C. Hahn, M. Rhee, and J.-E. Oh, "Effect of triggering on the energy absorption capacity of axially compressed aluminum tubes," *Materials & design*, vol. 20, no. 1, pp. 31–40, 1999.

[28] A. Mamalis, D. Manolakos, S. Saigal, G. Viegelahn, and W. Johnson, "Extensible plastic collapse of thin-wall frusta as energy absorbers," *International journal of mechanical sciences*, vol. 28, no. 4, pp. 219–229, 1986.

[29] G. Daneshi and S. Hosseinipour, "Grooves effect on crashworthiness characteristics of thin-walled tubes under axial compression," *Materials & design*, vol. 23, no. 7, pp. 611–617, 2002.

[30] S. Hosseinipour and G. Daneshi, "Energy absorbtion and mean crushing load of thin-walled grooved tubes under axial compression," *Thin-walled structures*, vol. 41, no. 1, pp. 31–46, 2003.

[31] N. Mamalis, B. Davis, C. D. Nilson, M. S. Hickman, and R. M. LeBoyer, "Complications of foldable intraocular lenses requiring explantation or secondary intervention—2003 survey update," *Journal of Cataract & Refractive Surgery*, vol. 30, no. 10, pp. 2209–2218, 2004.

[32] X. Zhang, H. Su, and T. Yu, "Energy absorption of an axially crushed square tube with a buckling initiator," *International Journal of Impact Engineering*, vol. 36, no. 3, pp. 402–417, 2009.

[33] T. Adachi, A. Tomiyama, W. Araki, and A. Yamaji, "Energy absorption of a thin-walled cylinder with ribs subjected to axial impact," *International journal of impact engineering*, vol. 35, no. 2, pp. 65–79, 2008.

[34] X. Zhang, G. Cheng, Z. You, and H. Zhang, "Energy absorption of axially compressed thin-walled square tubes with patterns," *Thin-Walled Structures*, vol. 45, no. 9, pp. 737–746, 2007.

[35] W. Abramowicz and T. Wierzbicki, "Axial crushing of multicorner sheet metal columns," *Journal of Applied Mechanics*, vol. 56, no. 1, pp. 113–120, 1989.

[36] A. Mamalis, D. Manolakos, A. Baldoukas, and G. Viegelahn, "Energy dissipation and associated failure modes when axially loading polygonal thin-walled cylinders," *Thin-Walled Structures*, vol. 12, no. 1, pp. 17–34, 1991.

[37] A. Mamalis, D. Manolakos, M. Ioannidis, P. Kostazos, and C. Dimitriou, "Finite element simulation of the axial collapse of metallic thin-walled tubes with octagonal cross-section," *Thin-Walled Structures*, vol. 41, no. 10, pp. 891–900, 2003.

[38] M. Yamashita, M. Gotoh, and Y. Sawairi, "Axial crush of hollow cylindrical structures with various polygonal cross-sections: Numerical simulation and experiment," *Journal of Materials Processing Technology*, vol. 140, no. 1-3, pp. 59–64, 2003.

[39] W. Chen and T. Wierzbicki, "Relative merits of single-cell, multi-cell and foam-filled thin-walled structures in energy absorption," *Thin-Walled Structures*, vol. 39, no. 4, pp. 287–306, 2001.

[40] C. G. H. Z. Zhang, X., "Theoretical prediction and numerical simulation of multi-cell square thin-walled structures," *Thin-Walled Structures*, vol. 44, no. 11, pp. 1185–1191, 2006.

[41] H.-S. Kim, "New extruded multi-cell aluminum profile for maximum crash energy absorption and weight efficiency," *Thin-Walled Structures*, vol. 40, no. 4, pp. 311–327, 2002.

[42] A. Mamalis and W. Johnson, "The quasi-static crumpling of thin-walled circular cylinders and frusta under axial compression," *International Journal of Mechanical Sciences*, vol. 25, no. 9-10, pp. 713–732, 1983.

[43] A. Aljawi and A. Alghamdi, "Investigation of axially compressed frusta as impact energy absorbers," *WIT Transactions on Engineering Sciences*, vol. 24, 1970.

[44] A. Mamalis, D. Manolakos, S. Saigal, G. Viegelahn, and W. Johnson, "Extensible plastic collapse of thin-wall frusta as energy absorbers," *International journal of mechanical sciences*, vol. 28, no. 4, pp. 219–229, 1986.

[45] S. R. Reid, T. Reddy, and M. Gray, "Static and dynamic axial crushing of foam-filled sheet metal tubes," *International Journal of Mechanical Sciences*, vol. 28, no. 5, pp. 295–322, 1986.

[46] S. Santosa and T. Wierzbicki, "Crash behavior of box columns filled with aluminum honeycomb or foam," *Computers & Structures*, vol. 68, no. 4, pp. 343–367, 1998.

[47] S. P. Santosa, T. Wierzbicki, A. G. Hanssen, and M. Langseth, "Experimental and numerical studies of foam-filled sections," *International Journal of Impact Engineering*, vol. 24, no. 5, pp. 509–534, 2000.

[48] M. Hanssen and O. S. Hopperstad, "Static and dynamic crushing of circular aluminium extrusions with aluminium foam filler," *International Journal of Impact Engineering*, vol. 24, no. 5, pp. 475–507, 2000.

[49] A. G. Hanssen, M. Langseth, and O. S. Hopperstad, "Static and dynamic crushing of circular aluminium extrusions with aluminium foam filler," *International Journal of Impact Engineering*, vol. 24, no. 5, pp. 475–507, 2000.

[50] A. Hanssen, M. Langseth, and O. Hopperstad, "Optimum design for energy absorption of square aluminium columns with aluminium foam filler," *International Journal of Mechanical Sciences*, vol. 43, no. 1, pp. 153–176, 2001.

[51] G. L. Farley and R. M. Jones, "Crushing characteristics of continuous fiber-reinforced composite tubes," *Journal of composite Materials*, vol. 26, no. 1, pp. 37–50, 1992.

[52] A. Mamalis, D. Manolakos, M. Ioannidis, and D. Papapostolou, "On the response of thin-walled cfrp composite tubular components subjected to static and dynamic axial compressive loading: experimental," *Composite structures*, vol. 69, no. 4, pp. 407–420, 2005.

[53] T. Wierzbicki *et al.*, "Axial resistance and energy absorption of externally reinforced metal tubes," *Composites Part B: Engineering*, vol. 27, no. 5, pp. 387–394, 1996.

[54] A. Mamalis, D. Manolakos, G. Demosthenous, and M. Ioannidis, "The static and dynamic axial crumbling of thin-walled fibreglass composite square tubes," *Composites Part B: Engineering*, vol. 28, no. 4, pp. 439–451, 1997.

[55] G. Sun, T. Pang, C. Xu, G. Zheng, and J. Song, "Energy absorption mechanics for variable thickness thin-walled structures," *Thin-Walled Structures*, vol. 118, pp. 214–228, 2017.

[56] P. Bandi, D. Detwiler, J. P. Schmiedeler, and A. Tovar, "Design of progressively folding thin-walled tubular components using compliant mechanism synthesis," *Thin-Walled Structures*, vol. 95, pp. 208–220, 2015.

[57] J. Song, Y. Chen, and G. Lu, "Axial crushing of thin-walled structures with origami patterns," *Thin-Walled Structures*, vol. 54, pp. 65–71, 2012.

[58] J. Ma and Z. You, "Energy absorption of thin-walled square tubes with a pre-folded origami pattern—part i: geometry and numerical simulation," *Journal of Applied Mechanics*, vol. 81, no. 1, p. 011003, 2014.

[59] J. Ma, D. Hou, Y. Chen, and Z. You, "Quasi-static axial crushing of thin-walled tubes with a kite-shape rigid origami pattern: numerical simulation," *Thin-Walled Structures*, vol. 100, pp. 38–47, 2016.

[60] N.-H. Kim, "Introduction to nonlinear finite element analysis," *Springer Science and Business Media*, vol. 1, pp. 1–73, 2014.

[61] T. Belytschko, W. K. Liu, B. Moran, and K. Elkhodary, "Nonlinear finite elements for continua and structures." *John wiley and sons*, vol. 2, pp. 227–312, 2013.

[62] LSTC, "Ls-dyna keyword user's manual," vol. 1, pp. 1–27, 2007.

[63] M. Ahmad, K. Ismail, and F. Mat, "Convergence of finite element model for crushing of a conical thin-walled tube," *Procedia Engineering*, vol. 53, pp. 586–593, 2013.

[64] A. Najafi, "Axial collapse of thin-walled, multi-corner single-and multi-cell tubes," *Masters Thesis, Mississippi State University*, 2009.

[65] P. Wriggers and G. Zavarise, "Computational contact mechanics," *Encyclopedia of computational mechanics*, vol. 498, pp. 24–60, 2004.

[66] LSTC, "Ls-dyna theory manual," vol. 1, pp. 1.10–1.14, 2006.

[67] S. Dong, A. Sheldon, K. Pydimarry, and M. Dapino, "Friction in ls-dyna®: Experimental characterization and modeling application," *14th International LS-DYNA Users Conference, Detroit, MI, USA*, pp. 3–12, 2016.

[68] S. P. Timoshenko and J. M. Gere, "Theory of elastic stability," *Courier Corporation*, vol. 2, pp. 46–178, 2009.

[69] K. U. Claussen, T. Scheibel, H.-W. Schmidt, and R. Giesa, "Polymer gradient materials: can nature teach us new tricks?" *Macromolecular Materials and Engineering*, vol. 297, no. 10, pp. 938–957, 2012.

[70] D. Jha, T. Kant, and R. Singh, "A critical review of recent research on functionally graded plates," *Composite Structures*, vol. 96, pp. 833–849, 2013.